iScience

CellPress
OPEN ACCESS

Article

T proliferating cells derived autophagy signature associated with prognosis and immunotherapy resistance in a pan-cancer analysis

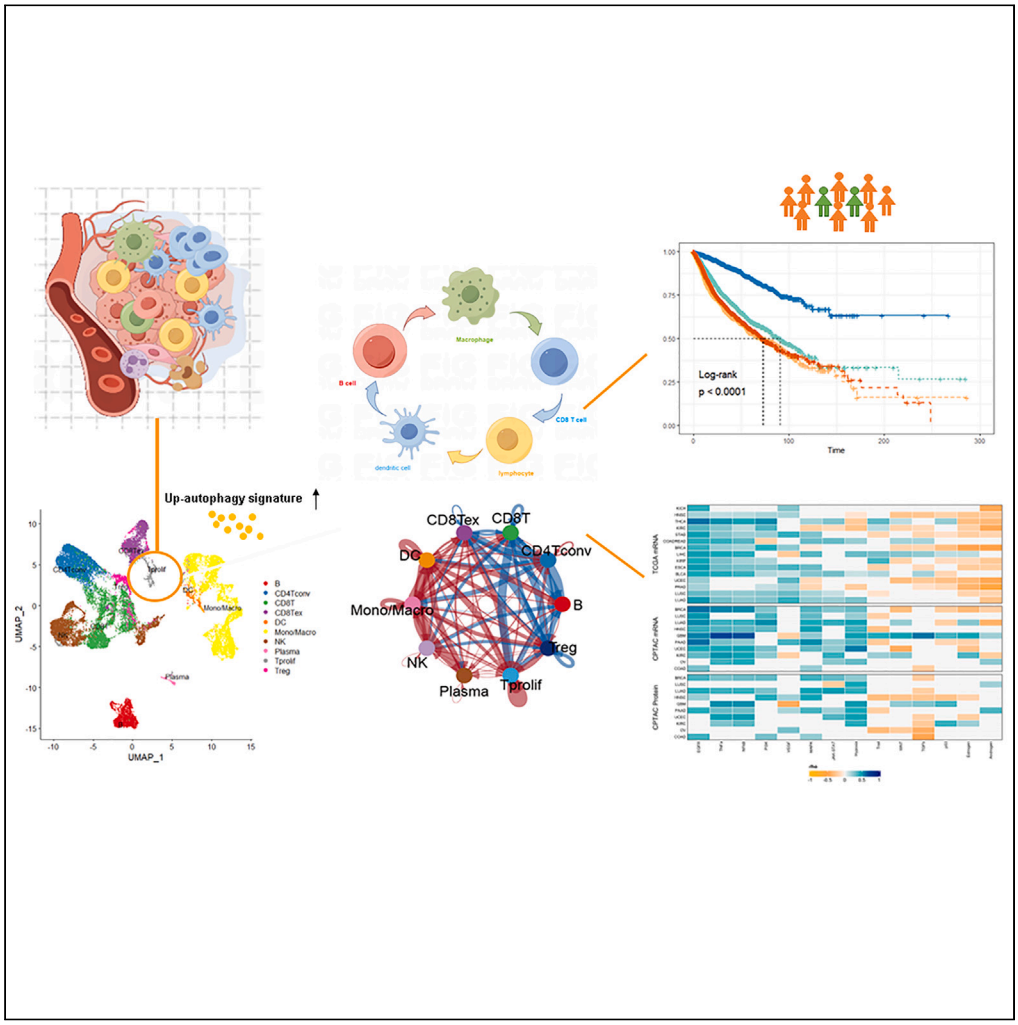

Zhongqi Fan, Yutao Liu, Chengcheng Li, ..., Shangli Cai, Tian Yang, Guoyue Lv

yangtianehbh@smmu.edu.cn (T.Y.)
lvgy@jlu.edu.cn (G.L.)

Highlights

We defined a T proliferating cell derived pan-cancer autophagy signature

Pan-cancer autophagy signature influences cell-cell interactions in TME

Pan-cancer autophagy signature predicts ICIs' responsiveness in multiple cancers

Metabolism inactivation accompanied with dysregulation of autophagy

Fan et al., iScience 27, 108701
January 19, 2024
https://doi.org/10.1016/j.isci.2023.108701

iScience

CellPress
OPEN ACCESS

Article

T proliferating cells derived autophagy signature associated with prognosis and immunotherapy resistance in a pan-cancer analysis

Zhongqi Fan,[1,7] Yutao Liu,[2,7] Chengcheng Li,[3,7] Yanfang Jiang,[4,7] Nanya Wang,[5,7] Mingda Wang,[6,7] Chao Li,[6] Yongkang Diao,[6] Wei Qiu,[1] Xin Zhu,[3] Guoqiang Wang,[3] Shangli Cai,[3] Tian Yang,[1,6,*] and Guoyue Lv[1,8,*]

SUMMARY

Despite autophagy modulating tumor immunity in the tumor microenvironment (TME), the immunotherapeutic efficacy and potential mechanism of autophagy signature was not explicit. We manually curated an autophagy gene set and defined a pan-cancer autophagy signature by comparing malignant tissues and normal tissues in The Cancer Genome Atlas (TCGA) cohort. The pan-cancer autophagy signature was derived from T proliferating cells as demonstrated in multiple single-cell RNA sequencing (scRNA-seq) datasets. The pan-cancer autophagy signature could influence the cell-cell interactions in the TME and predict the responsiveness of immune checkpoint inhibitors (ICIs) in the metastatic renal cell carcinoma, non-small cell lung cancer, bladder cancer, and melanoma cohorts. Metabolism inactivation accompanied with dysregulation of autophagy was investigated with transcriptomic and proteomic data. The immunotherapeutic predictive role and mechanism regulation of the autophagy signature was validated in an in-house cohort. Our study provides valuable insights into the mechanisms of ICI resistance.

INTRODUCTION

Autophagy, a key intracellular degradation process, can eliminate unnecessary or dysfunctional cellular components and recycle metabolic substrates. In response to stress signals in the tumor microenvironment (TME), the autophagy pathway can be modified in either tumor cells or immune cells, thus differentially influencing tumor progression, immunity, and therapy.[1,2]

Previous studies have demonstrated that autophagy influences the invasion and survival of cancer cells through both cell autonomous (directly impacting cancer cells) and non-autonomous (acting on other cells to determine the fate of cancer cells) mechanisms.[3] Tumor autonomous autophagy can affect the immune response of cancer cells, as secretory autophagy has been observed to decrease MHC-I-antigen complexes in pancreatic ductal adenocarcinoma (PDAC). Meanwhile, autophagy could non-autonomously shape the survival, activation, differentiation, and effector function of immune cell subsets in the TME.[4] Additionally, recent studies have demonstrated the involvement of the autophagy pathway in the trafficking of immune cell subsets in tumors.[4,5]

Although cumulative evidence indicated that autophagy may modulate tumor immunity through regulating various immune cells in the TME,[1,6] there are still several questions that remain to be characterized. These include: (1) the identification of autophagy-associated genes at the pan-cancer level, which play a predominant role in fueling tumor growth and facilitating immunomodulatory effects; (2) the classification of immune cell-derived or cancer intrinsic autophagy signatures; (3) the investigation of the immunotherapeutic efficacy of autophagy signatures, particularly in the context of cancer cohorts with large sample sizes; and (4) the exploration of the pathway regulation of autophagy in the TME.

Therefore, in this study, we defined a pan-cancer autophagy signature, mainly derived from the T proliferating cells, which influenced the prognosis and immunotherapeutic efficacy. Furthermore, the pan-cancer autophagy signature affected cell-cell interactions (CCIs) in the TME and could serve as a predictor for immunotherapeutic outcomes in multiple cancers. Furthermore, the inactivation of metabolism pathway accompanied by the dysregulation of autophagy was investigated using multiple cancer cohorts with transcriptomic and proteomic data.

[1]Department of Hepatobiliary and Pancreatic Surgery, General Surgery Center, First Hospital of Jilin University, Jilin, China
[2]State Key Laboratory of Molecular Oncology, Department of Medical Oncology, National Cancer Center/National Clinical Research Center for Cancer/Cancer Hospital, Chinese Academy of Medical Sciences and Peking Union Medical College, Beijing, China
[3]Burning Rock Biotech, Guangdong, China
[4]Key Laboratory of Organ Regeneration and Transplantation of the Ministry of Education, Genetic Diagnosis Centre, The First Hospital of Jilin University, Changchun, Jilin, China
[5]Phase I Clinical Trial Unit, First Hospital of Jilin University, Jilin, China
[6]Department of Hepatobiliary Surgery, Eastern Hepatobiliary Surgery Hospital, Second Military Medical University (Navy Medical University), Shanghai, China
[7]These authors contributed equally
[8]Lead contact
*Correspondence: yangtianehbh@smmu.edu.cn (T.Y.), lvgy@jlu.edu.cn (G.L.)
https://doi.org/10.1016/j.isci.2023.108701

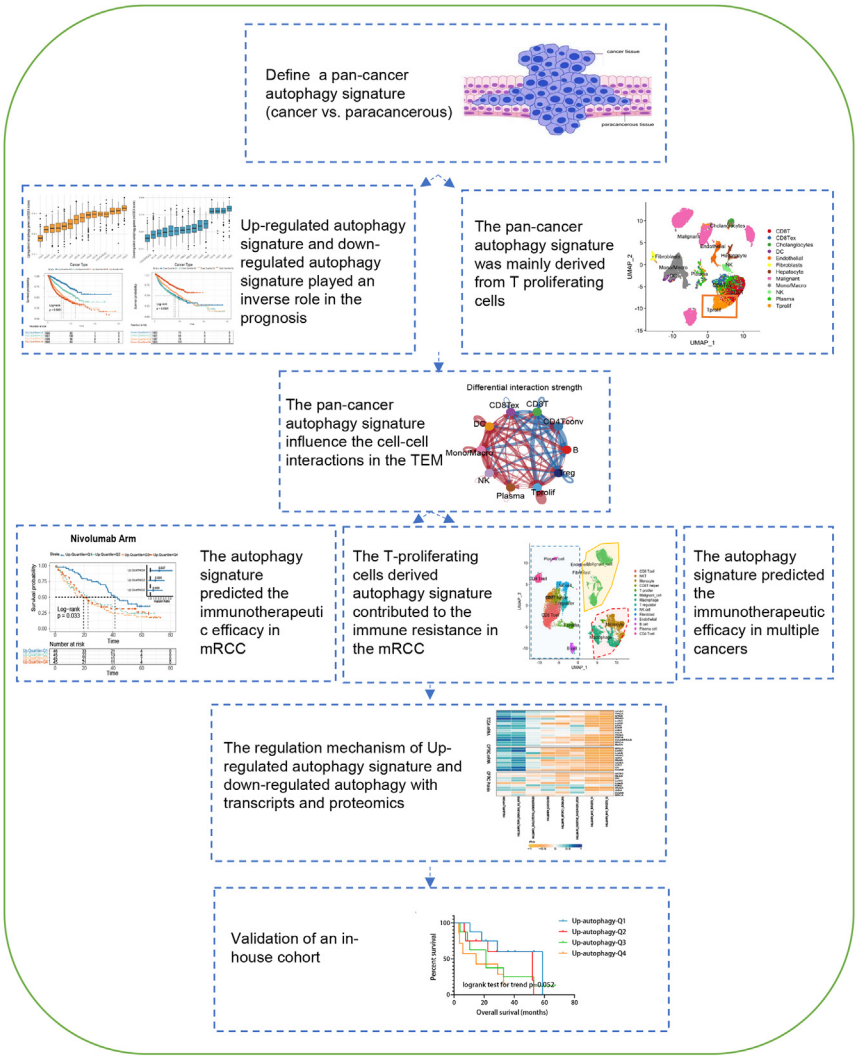

Figure 1. Flow chart of the study design

The immunotherapeutic predictive efficacy and mechanism regulation of autophagy signature was further validated in our in-house cohort. These findings provide valuable insights into the mechanisms of ICI resistance and could help inform strategies to overcome resistance to ICIs treatment.

RESULTS

Pan-cancer analysis of dysregulation in autophagy pathways

The flow chart of study design was shown as Figure 1. Initially, to classify the autophagy pathways, we manually curated a list of autophagy related genes by integrating published databases including Human Autophagy Database[7] (232 genes) and the Molecular Signatures Database (v4.0),[8] and previously published papers.[9,10] In total, we obtained 256 autophagy-related genes (Table S3). We defined a pan-cancer autophagy transcriptional signature to investigate the dysregulation in the autophagy pathway across different cancer types, due to the transcriptomic variability of the autophagy pathway across tissue types (Figure 2A; Figure S1A).

Subsequently, we identified 28 upregulated genes and 29 downregulated genes in the autophagy pathway by comparing malignant tissues and normal tissues in the TCGA cohort (USCS XENA portal: https://xena.ucsc.edu/) (limma-trend, FDR<0.05; Figure 2A; Figure S1B; Table S4). Given the transcriptomic variability of the autophagy pathway across tissue types (Figure 2A), ssGSEA was used to generate the up-autophagy and down-autophagy scores for up- and downregulated genes, respectively. The two scores showed a broad variation across tumor types (Figures 2C and 2D). Furthermore, distinct blocks of upregulated and downregulated genes were observed in clustering the Pearson correlation matrix of intergenic correlations across TCGA cancers (Figure 2B; Table S5, two-sided), suggesting co-regulation within the up- or downregulated genes respectively. Functional investigation revealed a crosslink between up-/down-autophagy signature and

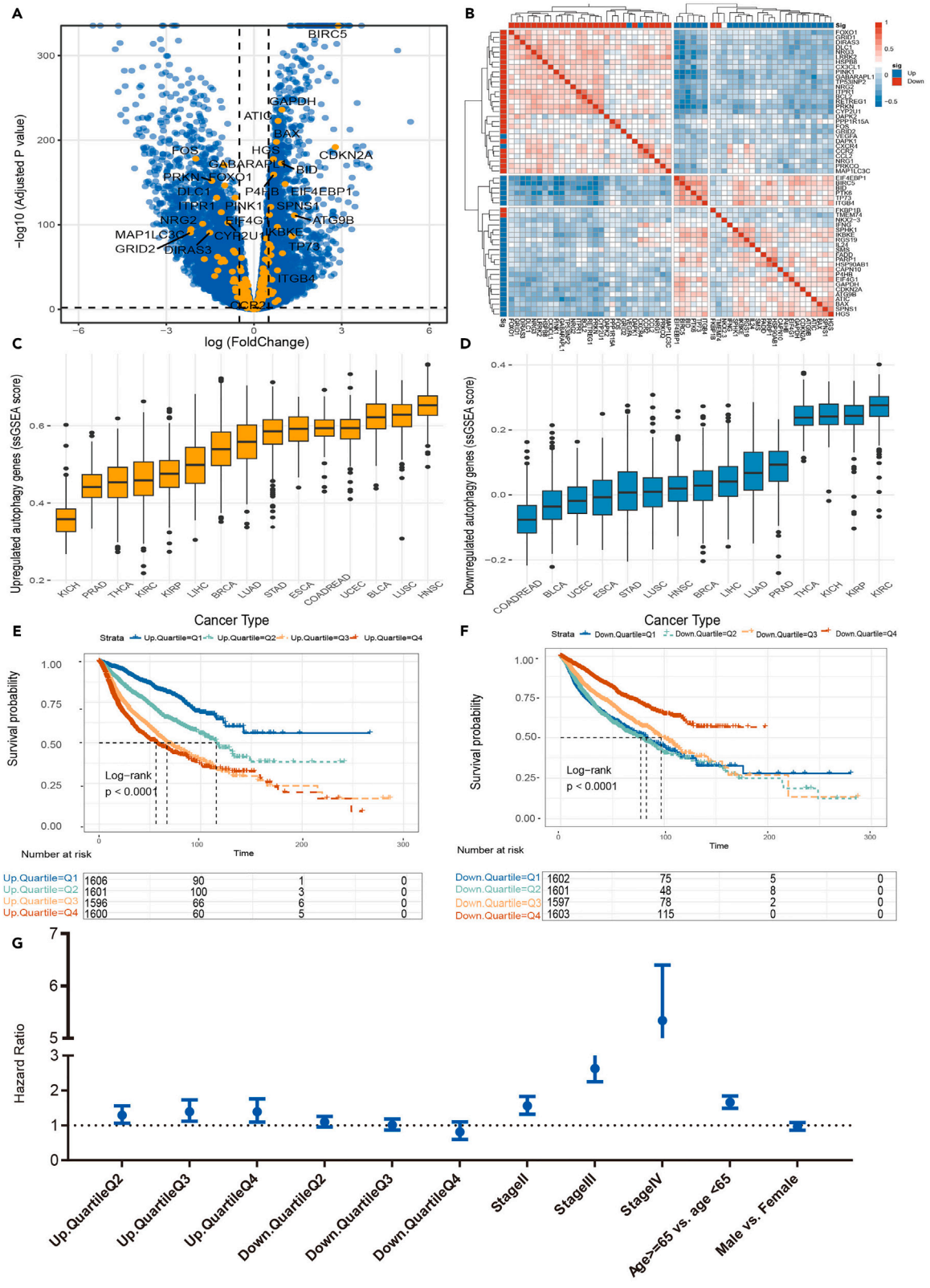
A
B
C
D
E
F
G
−log10 (Adjusted P value)
log (FoldChange)
BIRC5
GAPDH
ATIC
BAX
HGS
CDKN2A
FOS
GABARAPL1
BID
PRKN
FOXO1
DLC1
P4HB
EIF4EBP1
ITPR1
PINK1
SPNS1
NRG2
EIF4G1
ATG9B
MAP1LC3C
CYFIP2
IKBKE
GRID2
DIRAS3
TP73
ITGB4
CCR2
Upregulated autophagy genes (ssGSEA score)
Downregulated autophagy genes (ssGSEA score)
KICH
PRAD
THCA
KIRC
KIRP
LIHC
BRCA
LUAD
STAD
ESCA
COADREAD
UCEC
BLCA
LUSC
HNSC
Cancer Type
Strata
Up.Quartile=Q1
Up.Quartile=Q2
Up.Quartile=Q3
Up.Quartile=Q4
Down.Quartile=Q1
Down.Quartile=Q2
Down.Quartile=Q3
Down.Quartile=Q4
Survival probability
Log−rank
p < 0.0001
Number at risk
Time
Up.Quartile=Q1 1606 90 1 0
Up.Quartile=Q2 1601 100 3 0
Up.Quartile=Q3 1596 66 6 0
Up.Quartile=Q4 1600 60 5 0
Down.Quartile=Q1 1602 75 5 0
Down.Quartile=Q2 1601 48 8 0
Down.Quartile=Q3 1597 78 2 0
Down.Quartile=Q4 1603 115 0 0
Hazard Ratio
Up.QuartileQ2
Up.QuartileQ3
Up.QuartileQ4
Down.QuartileQ2
Down.QuartileQ3
Down.QuartileQ4
StageII
StageIII
StageIV
Age>=65 vs. age <65
Male vs. Female

Figure 2. Landscape of autophagy pathway in the pan-cancer and the association with the prognosis in TCGA cohort and CPTAC cohort

(A) Volcano plot showing fold changes for differentially expressed genes between cancerous tissues and adjacent normal tissues in the TCGA cohort. The genes in autophagy pathway were highlighted by orange points.

(B) The intergene Spearman's correlations among upregulated genes and downregulated genes of autophagy pathway between cancer and normal samples in the TCGA cohort.

(C and D) Boxplots of up-autophagy scores and down-autophagy scores in multiple cancer types of the TCGA cohort. Data are represented as mean ± SEM.

(E and F) Unadjusted Kaplan-Meier curves showing survival by the quartile of the up-autophagy or down-autophagy score. p value was calculated by the log rank test.

(G) Plot of multivariate Cox regression coefficients by the quartile of up-autophagy or down-autophagy score. p value was calculated by multivariable cox regression by adjusting the AJCC stages and cancer types (as statss), error bars indicate 95% confidence intervals (n = 6,128).

autophagy activation/inhibition at protein level. There was a positive correlation between up-autophagy and lapidate microtubule-associated protein 1A/1B-light chain 3A (LC3A)/LC3B expression, and a negative correlation between down-autophagy and LC3A/LC3B expression in multiple cancers in the CPTAC cohort (The omics database: http://www.linkedomics.org/login.php) with proteomics (Figures S1C and S1D. Rho >0, $p < 0.01$ for the up-scores, and Rho <0, $p < 0.01$ for the down-scores, Spearman's correlation). In addition, in the starvation-induced autophagy-activation cell-line model (GEO: GSE107600), a higher up-autophagy score was observed in the autophagy-activation group, and a higher down-autophagy score in the autophagy-inhibition group (Figures S1E and S1F t-test $p < 0.001$). Therefore, the results suggested that up-autophagy scores and down-autophagy scores were associated with autophagy activation and inhibition, respectively.

Pan-cancer autophagy signature was associated with the prognosis

The up-autophagy and down-autophagy scores were further segregated into quartiles (Q1–Q4) to investigate their prognostication, referring to the previous studies[11,12] to ensure the sample size is evenly distributed across groups. Patients with the lowest up-autophagy scores (bottom 25% quartile of up-autophagy score, Q1) had significantly longer overall survival (OS) than those with the highest up-autophagy scores (top 25% quartile of up-autophagy score, Q4) (Figure 2E, log rank $p < 0.001$). In contrast, patients with the lowest down-autophagy scores (bottom 25% quartile of down-autophagy score, Q1) showed an increased risk of death compared to those with the highest down-autophagy scores (top 25% quartile of down-autophagy score, Q4) (Figure 2F, log rank $p < 0.001$). Multivariable Cox regression was used to examine the prognostic role of up- and down-autophagy score quartiles in the TCGA cohort, along with clinical covariates including age, sex, and American Joint Committee on Cancer stages, meanwhile, the tumor type was included as strata. The up-autophagy scores were still significantly associated with a worse prognosis. (HR = 1.73, $p < 0.05$ for Q4 vs. Q1 for the up-autophagy score; HR = 0.73, $p < 0.05$ for Q4 vs. Q1 quartile for the down-autophagy score, Cox regression; Figure 2G). In the subgroup analysis, we consistently observed the converse prognostication regardless of the stage (stage I-II or stage III-IV) (Figures S2A and S2B), or in most individual cancer types (Figure S2C). These results suggested that the dysregulated autophagy-related genes were clinically relevant and up-autophagy and down-autophagy score had opposite prognostic roles in cancers.

Pan-cancer autophagy signature was a property of T proliferating cells

Although autophagy could be extensively induced in various cell types, different cells may exert a distinct role in determining the biological function of autophagy.[1] To determine the cell origin of the pan-cancer autophagy signature, we performed multi-omics analysis. Initially, we determined the correlations between the up- or down-autophagy scores and estimated purity. Because if the autophagy signature came from the tumor epithelial compartment and it would be a positive association with tumor cellularity.[11] As a result, the up- and down-autophagy scores were both negatively correlated with tumor purity, which was independently estimated by the allele-specific copy number profiles using, ABSOLUTE,[13] ASCAT,[14] AbsCN-seq,[15] PurBayes,[16] CPE[3] and ESTIMATE,[17] respectively (Figures 3A and 3B; Table S6). Besides, we consistently observed the negative correlations between the up- and down-autophagy scores and the median variant allele frequency (VAF) (Rho = 0.05, $p = 0.30$ for the up-scores, and Rho = −0.30, $p < 2.2e\text{-}16$ for the down-scores, Spearman's correlation, Figure 3C), and the frequency of cancer cells (Rho = −0.33, $p < 2.2e\text{-}16$ for the up-autophagy scores; Rho = −0.15, $p < 2.2e\text{-}16$ for the down-autophagy scores, Spearman's correlation, Figure 3D), which was evaluated by genomic variation and methylation-based deconvolution approach,[18] respectively. Moreover, no correlation between up- and down-autophagy scores and the tumor specific mRNA (TmS) (Rho = −0.07, $p = 0.82$ for the up-scores, and Rho = −0.33, $p = 0.39$ for the down-scores, Spearman's correlation, Figure 3E), which represented the total mRNA transcript level per haploid genome of specific tumor cells.[19] Collectively, these results from multi-omics perspective suggested the pan-cancer autophagy signature was not the cancer intrinsic property.

In parallel, we observed positive correlations between immune cells and autophagy signature (up-autophagy score and down-autophagy score), including CD8+T cell, $CD14^+$ monocytes, $CD56^+$ macrophage deconvoluted by TIMER2[20] algorithm (Figures S3A and S3B; Table S7), and positive correlations between autophagy signature and known marker genes for the cytolytic activity (CYT) (geometric mean of *GZMA* and *PRF1*),[21] CD8 T cells (*CD8A* expression), monocytes (*CD14* expression) and CAFs (*ACTA2* expression)[22] (Figure S3C), suggesting that the pan-cancer autophagy signature was immune-cell-originated features. Given the distinct role of different immune cells in impacting autophagy modulation, we then tried to determine the potential cell types associated with transcriptional variations of the autophagy pathway. In the subsequent analysis, four types of cancers, including RCC (GEO: GSE121636),[23] KIRC (GEO: GSE139555),[24] CHOL (GEO: GSE138709),[25] and CRC (GEO: GSE134520),[26] were studied using available scRNA-seq data. The cells were separated into cancer, stromal, or immune cells of origin using cell sorting technology at high resolution (Figures 3F–3I).

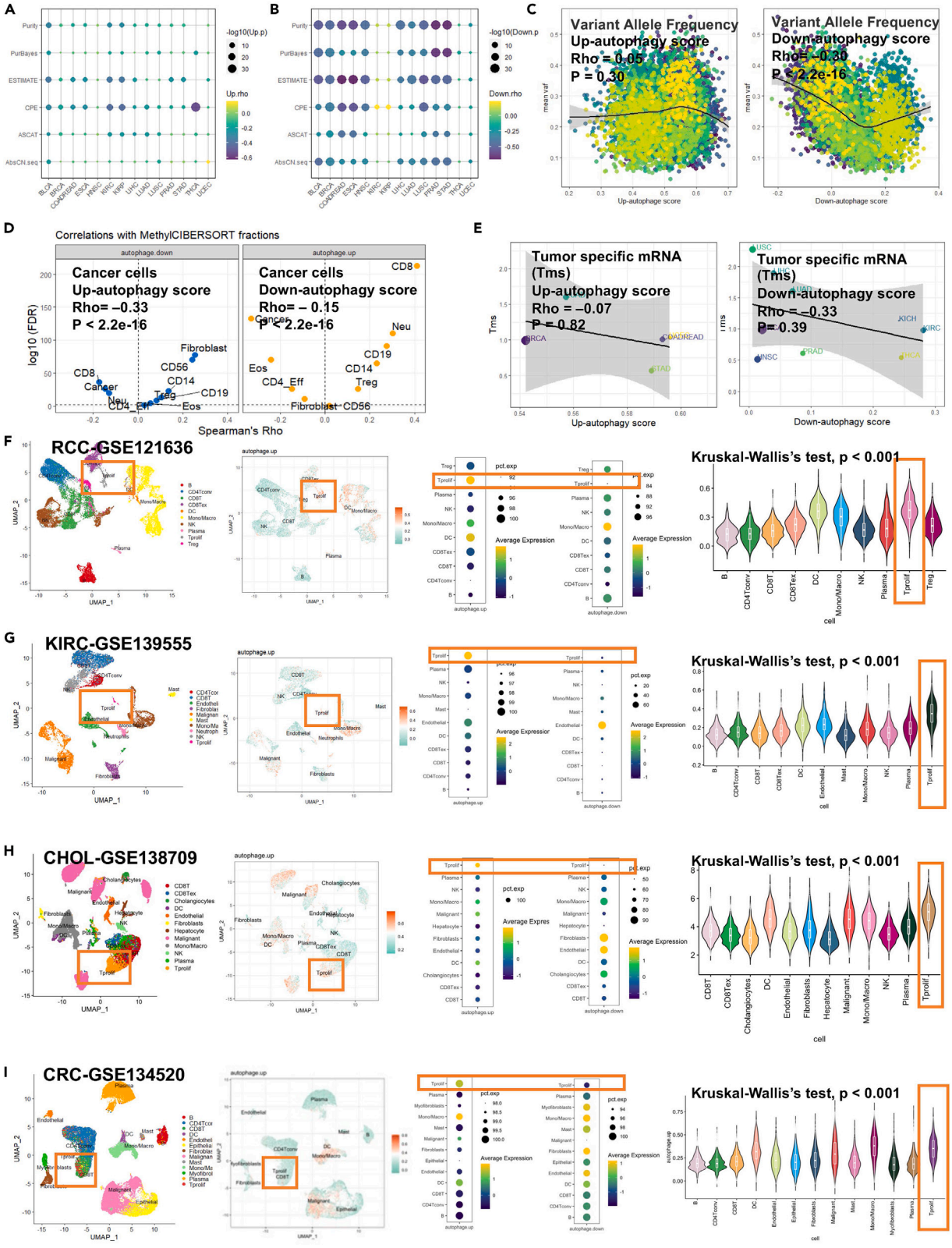
A
B
C
Variant Allele Frequency
Up-autophagy score
Rho = 0.05
P = 0.30
Variant Allele Frequency
Down-autophagy score
Rho = −0.30
P < 2.2e-16
Up-autophage score
Down-autophage score
D
Correlations with MethylCIBERSORT fractions
autophage.down
autophage.up
Cancer cells
Up-autophagy score
Rho= −0.33
P < 2.2e-16
Cancer cells
Down-autophagy score
Rho= − 0.15
P < 2.2e-16
log10 (FDR)
Spearman's Rho
E
Tumor specific mRNA
(Tms)
Up-autophagy score
Rho = −0.07
P = 0.82
Tumor specific mRNA
(Tms)
Down-autophagy score
Rho = −0.33
P = 0.39
Tms
Up-autophage score
Down-autophage score
F
RCC-GSE121636
Kruskal-Wallis's test, p < 0.001
G
KIRC-GSE139555
Kruskal-Wallis's test, p < 0.001
H
CHOL-GSE138709
Kruskal-Wallis's test, p < 0.001
I
CRC-GSE134520
Kruskal-Wallis's test, p < 0.001
cell

Figure 3. The cell origin of upregulated or downregulated autophagy genes

(A and B) Positive or inverse correlations between up-and down-autophagy scores and purity estimated by ABOSLUTE, PurBayes, ESTIMATE, CPE, ASCAT, and AbsCN.seq.

(C–E) Positive or inverse correlations between up-autophagy scores or down-autophagy scores and mean VAF, cell deconvolution by MethyCIBERSORT and total cancer specific mRNA.

(F–I) The up-autophagy and down-autophagy scores in different cell types in the RCC dataset, KIRC dataset, CHOL dataset, CRC dataset. Data are represented as mean ± SEM. Note: Different cancer types were marked by different colors for (C).

Consistently, we observed that the up-autophagy score exhibited significantly higher expression in the T proliferating cells and dendritic cells, compared with other immune cells (CD8T cells, NK cells, mast cells, mono/macrophage cells, plasma cells etc.), or the stromal cells (fibroblast and endothelial cells), as well as the malignant cancer cells in multiple datasets (Figures 3F–3I, Kruskal-Wallis's test, $p < 0.001$). In all the scRNA-seq datasets, the up-autophagy signature was predominantly expressed in the T proliferating cells (Figures 3F–3I, Kruskal-Wallis's test, $p < 0.001$). In contrast, the down-autophagy scores were associated with relatively lower expression in the T proliferating cells compared with other cells (Figures 3F–3I), suggesting that T proliferating cell population was one of the main sources for the pan-cancer autophagy signature. Finally, we also performed statistical testing for T proliferating cells-association for each up- or downregulated autophagy genes in these scRNA-seq datasets and found that most of upregulated autophagy genes were significantly overexpressed (mean difference >0, FDR <0.05, Wilcoxon's Rank-Sum Test; Figures S3D–S3I) and the majority of the downregulated autophagy genes were significantly under-expressed in the T proliferating cells compared to other cell types including other immune cells, stromal cells and malignant cells (mean difference <0, FDR <0.05, Wilcoxon's Rank-Sum Test; Figures S3D–S3I).

Altogether, these results supported that the pan-cancer autophagy signature was T proliferating cell origin, rather than stromal cell and cancer cells origin, as a general feature of malignancy.

Pan-cancer autophagy associated with pan-cancer prognosis independent of T proliferating cell signature

Above results suggested the pan-cancer autophagy signature was mainly derived from immune cells, particularly T proliferating cells (characterized by high expression of cell cycle-related genes, such as *MKI67* and *TOP2A*).[27] Previous studies have shown that T cells had diverse activation states, including naivete, cytotoxicity, exhaustion, and proliferation states, which may contribute to distinct anti-tumor killing effect.[28] While T exhausted cells expressed several exhaustion and dysfunction markers (e.g., *CTLA4, PDCD1, TIGIT, LAG3, LAYN* and *HAVCR2*),[27,28] which was associated with the inactivation of CD8 T cells in several cancers. On the other hand, cytotoxic CD8 + T-lymphocytes cells, with the activation of *GZMA/B, IFNG, NKG7, PRF1, CXCL13* and *GNLY*,[27] played an important role in anti-tumor immunity. Pseudo-time analysis identified dynamically T cells subsets differentiation trajectory (Figure S4A), and suggested T proliferating cells may be the precursor of T exhausted cells (Figure S4B), which is in line with recent studies that T proliferating cells represented a pre-exhausted state.[29]

To determine the distinct prognostication of T cell subsets, we integrative analyzed the ssGSEA score of T-proliferating cell signature and T-cytotoxic cell signature (*GZMA/B, PRF1, NKG7, IFNG, GNLY* and *CXCL13*),[28] which were segregated into quartiles (Q1–Q4). Patients with the lowest T-proliferating cell scores (Q1) had significantly longer overall survival (OS) than those with the highest T-proliferating cell scores (Q4) (Figure 4A, log rank $p < 0.001$) in the TCGA cohort, which was opposite to the prognostic role of T-cytotoxic cell signature (Figure 4B), suggested the T proliferating cell and T cytotoxic cell displayed an opposite T cell responsiveness.

Given the poor prognostic role of T proliferating cells per se, we were wondering whether it was that the T proliferating cells rather than the autophagy signature itself, that contributed to the worse prognostication. As a result, even though the up-autophagy scores had a strong positive correlation with the T proliferating cells (Figure 4C, Rho = 0.71, $p < 2.2e\text{-}16$, Spearman's correlation), the up-autophagy scores remained significantly associated with inferior prognosis in the multivariable Cox regression, after adjusting for T-proliferating cell signature scores, T-cytotoxic cell signature scores, and other clinical covariates, such as age, sex, clinical stage, and the tumor type (as strata) (Figure 4D). In the subgroup analysis, we consistently observed the conversely prognostication in both the high T-proliferating cell scores (Q4) group and the low T-proliferating cell scores (Q1) group (Figures 4E and 4F, log rank $p < 0.05$), suggesting that the pan-cancer autophagy signature influenced the pan-cancer prognosis independent of the T proliferating cell signature.

Pan-cancer autophagy signature affect cell-cell interactions in the immune microenvironment

Cell-cell interactions (CCIs) play an important role in cellular differentiation and homeostasis.[30] Since we demonstrated the up- and down-regulated autophagy genes were mainly derived from the T proliferating cells above. To further identify possible non-cell-autonomous effects in determining the fate of cancer cells, CellChat was used to identify putative signaling between different cell populations via known receptor-ligand pairs.[31] T proliferating cell populations showed strong interactions with dendritic cells (DCs), Mono/Macrophage and T exhausted cells than other cells regarding the number or strength/weights of interactions in multiple types of cancers (Figures 5A–5E), partly in line with the distribution of upregulated autophagy signature in the TME (Figures 3F and 3I).

Previous study reported that deletion of specific autophagy-related genes induced differentiation of activated T cells into regulatory, memory or natural killer T cells.[32] To further identify the potential non-cell-autonomous interaction mediated by the upregulated autophagy signature, we analyzed the alterations of CCIs between high up-autophagy score (Q4) and low up-autophagy score (Q1). Q4 had an increased number and strength of inferred interactions compared with Q1, especially the interactions between T proliferating cells and T exhausted

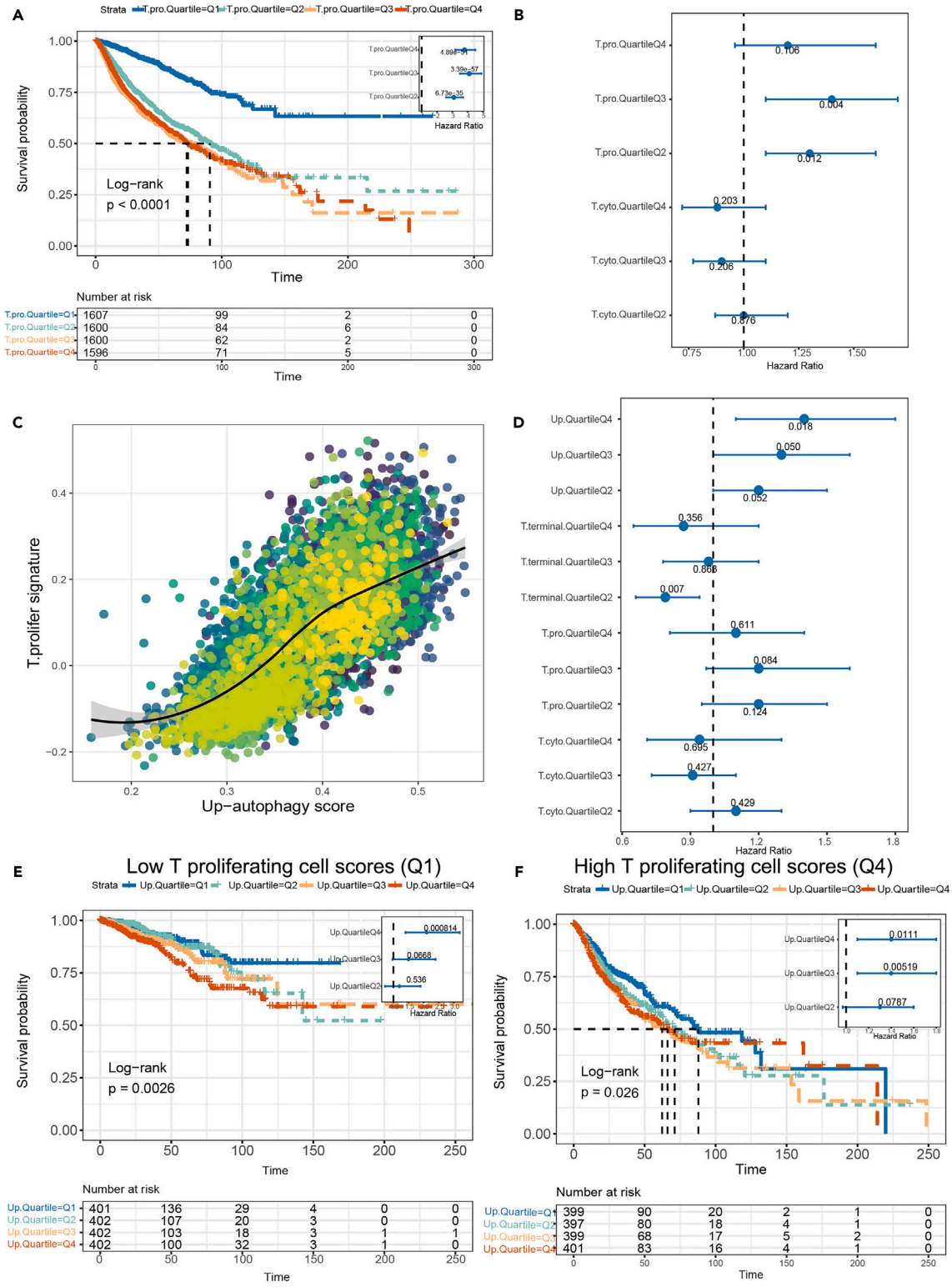

Figure 4. Pan-cancer autophagy signature influence the prognosis independent of T proliferating cell signature

(A) Unadjusted Kaplan-Meier curves showing survival by the quartile of the T proliferating cell score. p value was calculated by the log rank test.

(B) Plot of multivariate Cox regression coefficients by the T proliferating cell score and T cytotoxic cells signature score. p value was calculated by cox regression by adjusting the stages and tumor types, error bars indicate 95% confidence intervals (n = 6,128).

Figure 4. *Continued*

(C) Spearman's correlations between up-autophagy scores and the T proliferating cell scores. Different cancer types were marked by different colors.

(D) Plot of multivariate Cox regression coefficients by the T proliferating cell score, T cytotoxic cells signature score, T terminal cells signature score, and Up-autophagy score. p value was calculated by cox regression by adjusting the stages and tumor types, error bars indicate 95% confidence intervals (n = 6,128).

(E and F) Kaplan-Meier curves showing survival by the quartile of the up-autophagy in the 4th quartile of the T proliferating cell score and in the 1st quartile of the T proliferating cell score. p value was calculated by the log rank test.

cells or T regulated cells (Figures 5F–5H; Figures S5A–S5C), while the two latter cells exerted negative regulatory effect on anti-tumor immunity to favor tumor development. In contrast, the interactions between T proliferating cells and T cytotoxic cells were decreased in the Q4 group compared with the Q1 group (Figures 5F–H), indicating that the high up-autophagy score may mediate the T cell differentiation and tumor-killing effect.

Signaling changes between Q1 and Q4 group were also observed, and multiple signaling including CCL-CCR, IFNG (IFNG-IFNGR1/2), IL16-CD4, FASL-FAS, TNFSF9-TNFRSF9, MIF(CD74-CXCR4), were significantly increased in the Q4 group between CD8 exhausted cells and other cells, such as T proliferating cells, T regulator cells, monocytes, and macrophages (Figures 5I; Figures S5D and S5E). In parallel, we also observed an increase in the relative information flow from Q1 to Q4 with respect to IFNγ, TNFα, CCL, CXCL, TGFβ, Fas signaling, etc (Figures 5J; Figures S5F and S5G).

Overall, these results suggested that the up-autophagy signature was involved in the T cell differentiation and T cell mediated anti-tumor immunity. It suggested the possibility of complex regulation mediated by the up-autophagy signature, providing insights into non-cell-autonomous effects of the autophagy in the TME and potential influence of the immunotherapeutic efficacy eventually.

Pan-cancer autophagy signature was associated with the efficacy of anti-PD-1/PD-L1 antibody in the mRCC cohort

Based on the above findings, we were motivated to investigate the immunotherapeutic efficacy of the up- or downregulated autophagy signature given autophagy involved in the CCIs among immune cells in the TME.

We observed the gradually increased survival from the bottom quartile (Q1) to the top quartile (Q4) of the up-autophagy scores (HR = 1.80, p = 0.037 for top vs. bottom quartile, Cox regression; Figure 6A) in the patients with mRCC who received anti-PD1/anti-PD-L1 regimens, while the down-autophagy scores played the inverse role in predicting the immunotherapeutic efficacy (HR = 0.75, p = 0.05 for top vs. bottom quartile, Cox regression; Figure 6B). The higher T proliferating cell score was associated with inferior immunotherapeutic outcomes (HR = 1.30, p = 0.015 for top vs. bottom quartile, Cox regression; Figure 6C), in agreement with the predictive efficacy of the up-autophagy score.

The mutation frequencies of *PBRM1* were balanced among Q1 to Q4 of the up-autophagy score, while the Q1 had a relatively lower frequency of *SETD2* and *BAP1* mutations compared with Q4 (Chi-square test, $p < 0.05$) (Figure 6D). In the multivariable cox regression, the up-autophagy score remained significantly associated with the survival in patients treated with anti-PD1/anti-PD-L1 regimens by adjusting age, sex, T proliferating cell signature scores and gene mutations (Table S8). These results suggested that the up-autophagy signature independently influenced the immunotherapeutic effect in the patients with mRCC.

We further explored whether the up-autophagy score was associated with treatment choice-decision in the patients with mRCC. In contrast, the up-autophagy and down-autophagy scores were not associated with the therapeutic benefit from everolimus (Log rank, p = 0.47 for the up-autophagy score, p = 0.18 for the down-autophagy score; Figures S6A and S6B), an mTOR inhibitor, suggesting its specific immunotherapeutic predictive power of the autophagy scores. Furthermore, in the bottom quartile of the up-autophagy scores (Q1) group, patients who received anti-PD-1 antibody had a longer overall survival than those who were treated with everolimus (log rank $p < 0.001$, HR = 0.55, 95% CI, 0.31–0.95. Figure 6E), while the out-performance of anti-PD-1 over everolimus was abrogated in the Q4 group (log rank p = 0.67; HR, 0.90, 95% CI: 0.54–1.50; Figure 6F). To further validate the conclusion, we analyzed another independent mRCC cohort who were treated with anti-PD1/anti-PD-L1 regimens or anti-angiogenic therapy (axitinib), the result was further confirmed, that in the bottom quartile of the up-autophagy scores (Q1) group, patients who received anti-PD-1 antibody had a longer PFS than those who were treated with axitinib (log rank p = 0.016, HR = 0.41, 95% CI, 0.24–0.70. Figure 6G), while the out-performance of anti-PD-1 over axitinib was not observed in Q4 group (log rank p = 0.85; HR, 0.84, 95% CI: 0.50–1.42; Figure 6H). These results suggested the up-signature predicted a superior outcome of anti-PD-1 antibody over the targeted therapy, indicating the potential to guide treatment choice-decision in the clinic for mRCC, although further validation with the perspective clinical trial is warranted.

To further uncover the mechanism, we first investigated the co-occurrence of up-autophagy score and the established immunotherapeutic predictive biomarkers. In the mRCC immunotherapy cohort, we observed that the up or down-autophagy scores were not correlated with tumor mutation burden (TMB) (Up-autophagy, Rho = −0.11, p = 0.21; Down-autophagy, Rho = 0.20, p = −0.12, Spearman's correlation) and neoantigens (Up-autophagy, Rho = −0.13, p = 0.15; Down-autophagy, Rho = −0.15, p = 0.09, Spearman's correlation, Figures S5C and S5D). Additionally, the $CD8^+$ T cell counts at the tumor margin or at the tumor center at protein level by immunofluorescence detection were not correlated with the up-or down-autophagy scores (Figure S6E) in the mRCC immunotherapy arm, and there were no significant differences of up- or down autophagy scores among three immune phenotypes including immune infiltrated, immune desert and immune excluded phenotype defined previously[33] (Kruskal-Wallis's test, p = 0.26 for up-autophagy score, p = 0.65 for down-autophagy score; Figure S6F). These results suggested the pan-autophagy signature did not interfere with the established biomarkers.

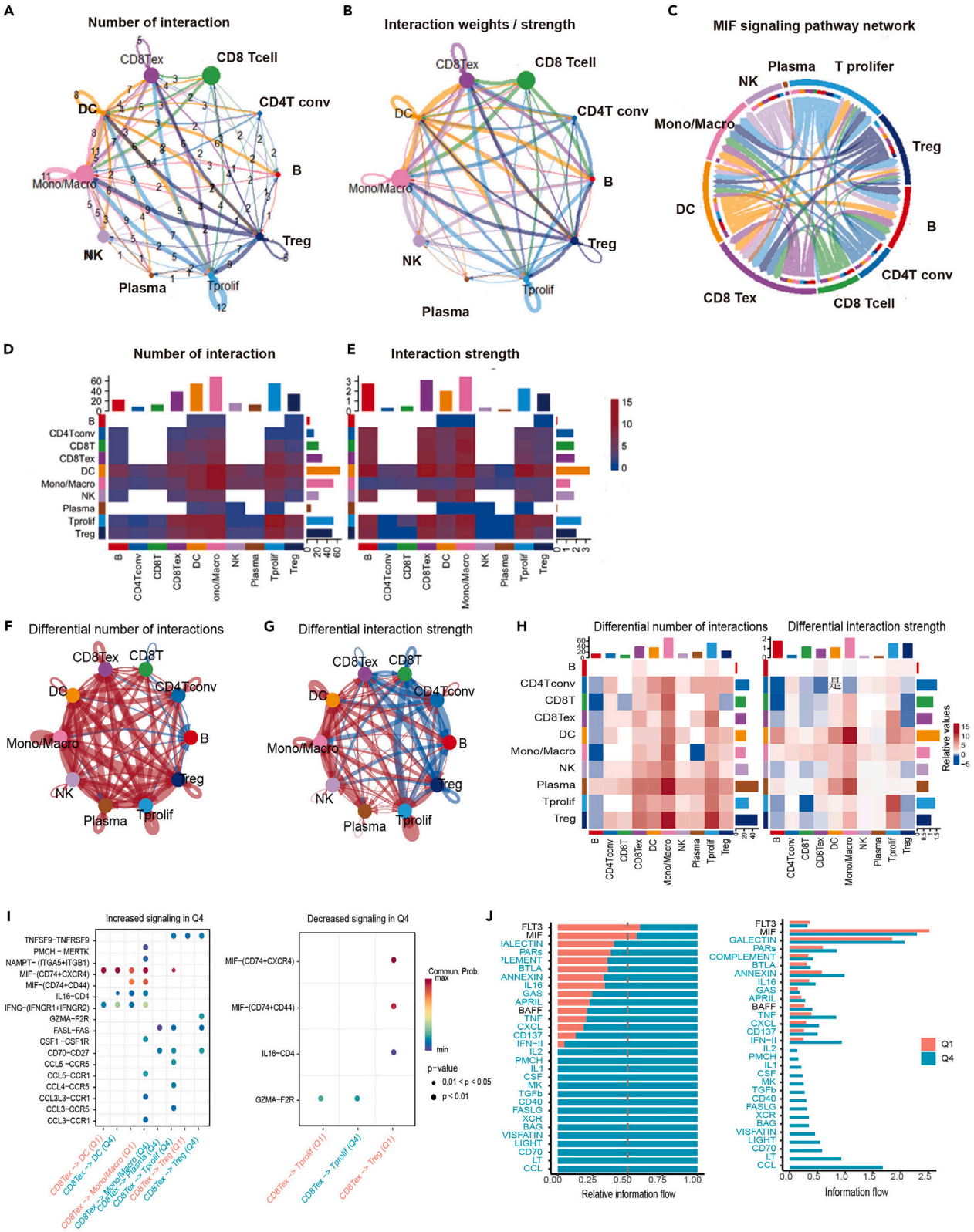
A
Number of interaction
CD8Tex
CD8 Tcell
CD4T conv
B
Treg
Tprolif
Plasma
NK
Mono/Macro
DC
B
Interaction weights / strength
C
MIF signaling pathway network
Plasma
T prolifer
NK
Mono/Macro
Treg
DC
B
CD4T conv
CD8 Tex
CD8 Tcell
D
Number of interaction
E
Interaction strength
B
CD4Tconv
CD8T
CD8Tex
DC
Mono/Macro
NK
Plasma
Tprolif
Treg
F
Differential number of interactions
G
Differential interaction strength
H
Differential number of interactions
Differential interaction strength
Relative values
I
Increased signaling in Q4
Decreased signaling in Q4
Commun. Prob.
max
min
p-value
0.01 < p < 0.05
p < 0.01
J
Relative information flow
Information flow
Q1
Q4

Figure 5. Pan-cancer autophagy signature effects cell-cell interactions in the immune microenvironment

(A and B) The number and weights/strength of interactions among different cell types in the mRCC scRNA-seq dataset.

(C) MIF signaling pathway network depicting the interactions among different cell types in the mRCC scRNA-seq dataset.

(D and E) Heatmap plot illustrating the number and strength of interactions among different cell types in the mRCC scRNA-seq dataset.

(F and G) The number and strength of interactions in different cell types between 1st (Q1) and 4th quartile (Q4) of up-autophagy score in the mRCC scRNA-seq dataset. Compared with Q1, red represents the number and strength of interactions were strengthened, and blue represents the number and strength of interactions were decreased.

(H) Heatmap plot illustrating the number and strength of interactions in different cell types between 1st (Q1) and 4th quartile (Q4) of up-autophagy score in the mRCC scRNA-seq dataset.

(I) The increased or decreased signaling in the 4th quartile (Q4) of up-autophagy score compared with 1st quartile (Q1) of up-autophagy score.

(J) The relative information flow from Q1 to Q4 with respect to IFNγ, TNFα, CCL, CXCL, TGFβ, Fas signaling.

Immune cell instead of cancer cell derived autophagy signature contributes to the ICI resistance in mRCC

Given that the autophagy signature was mainly immune cell driven, we further explored cell types contributing to the ICI resistance in a mRCC scRNA-seq cohort (GSE115978, anti-PD-L1 antibody, n = 25), which separated the malignant cells and immune cells by the flow cytometry. The cell type was annotated by integrating their functional marker expression (Figure 7A; Figures S7A–S7C) and the original published paper (Figure S6D). The scRNA-seq of mRCC was performed in the baseline. Consistent with the above result, the up-autophagy signature was higher in the T proliferating cells (Figures S7E and S7F). Moreover, the up-autophagy scores were higher in the T proliferating cells of the ICI-responders than that of the ICI-non-responders (Mann-Whitney test $p < 0.001$; Figure 7B), and the-down-autophagy scores were lower in the T proliferating cells of the ICI-responders than that of the ICI-naïve (non-ICI) and ICI-non-responders (Mann-Whitney test $p < 0.001$; Figure 7B). Although we observed the significantly increase of the up-autophagy scores in the responders of ICI in the B cells, Monocyte/Macrophage cells and malignant cells compared with the non-responders, the low-autophagy score was also increased in the responders of ICI in the B cells and malignant cells. In contrast, the down-autophagy scores displayed no significant differences between ICI-responders and ICI-naive and ICI-non-responders in Monocyte/Macrophage, B cells and the malignant cells (Figure 7C). This suggests that it is the T-proliferating cell derived up-autophagy signature that contributed to the ICI-resistance, given that the up-autophagy score was predominately expressed in the T proliferating cells simultaneously (Figures 3F–3I).

To further exclude the cancer cell-intrinsic contribution of the up-autophagy signature to ICI resistance, we used the previously established clear cell renal cancer cell line (Renca)[34] and CRC cell line (CT26) model[35] (TISMO database: GSE1394767, GSE153941) given that the transcriptome of these cancer cells were sequenced before transplantation, and would not be contaminated by the immune cell infiltration of the recipient mice. The two cancer cell lines were expanded *in vitro* and then transplanted into syngeneic recipient BALB/cArc or Balb/c mice. The recipient mice were then treated with anti-CLTA4/anti-PD-1, control IgG, or anti-PD-1, respectively, and the responders and non-responders of ICI treatment were identified (see STAR methods). As expected, there were no significant differences of the up-autophagy scores and down-autophagy scores in the ICI-non-responders and the ICI-responders (One-way ANOVA test $p = 0.46$; Figures 7E and 7F), indicating that it was not the cancer intrinsic program that contributed to immunosuppression.

Taken together, all the above results suggested that it was the immune cell derived instead of cancer-intrinsic up-autophagy signature that contributed to the ICI resistance.

Pan-cancer up-autophagy signature was associated with anti-PD-1/PD-L1 antibody failure in multiple immunotherapeutic cohorts

We were motivated to investigate the immunotherapeutic efficacy of the up-autophagy score in other immunotherapeutic cohorts, focusing on those studies that received anti-PD1/anti-PD-L1 regimens, which reinvigorated the dysfunctional tumor-infiltrating $CD8^+$ T cells.[36]

To comprehensive evaluate the immunotherapeutic efficacy of the up- or downregulated autophagy genes, we do the nonnegative matrix factorization (NMF) clustering based on these genes in the immunotherapeutic arm in mRCC (n = 181, anti-PD1 antibody). This analysis revealed four distinct subtypes, denoted group I–IV in mRCC (Figures S9A–S9C), with a relative high expression of up-autophagy score in group I in mRCC (Figure S9C), and relatively low down-autophagy score in group IV (Figure S9C), Classification using the up- or downregulated autophagy genes revealed four subtypes with distinct therapeutic outcomes (Figure S9D).

The distinct therapeutic outcomes were further observed in the BLCA (n = 348, anti-PDL1 antibody, Figure S9E), NSCLC (n = 130, anti-PD(L)1 antibody, Figure S9I) and melanoma-A (n = 121, anti-PD1 antibody, Figure S9M) and melanoma-B (n = 41, anti-PD1 antibody, Figure S9Q) cohorts. Similarly, the up-autophagy score was higher in group I in BLCA (Figure S9G) and NSCLC (Figure S8K), and the down-autophagy score was lower in group IV in BLCA, NSCLC, melanoma-A/B (Figures S9H, S9L, S9P, and S9T) cohorts. Classification using the up- or down-regulated autophagy genes revealed four subtypes with distinct therapeutic outcomes (Figures S9A, S9E, S9I, S9M, and S9Q), although the gene expression patterns were not identical, suggesting that the gene function in the autophagy signature is not the same across different cancers (Figures S9B, S9F, S9J, S9N, and S9R).

Association between the pan-cancer autophagy signature and cancer pathways

We first comprehensively calculated the pathways accompanied by the up- or down-autophagy signatures in the bulk RNA sequencing, and then observed multiple metabolic signaling alterations based on the KEGG gene sets (n = 186) in the TCGA and the CPTAC cohort. We

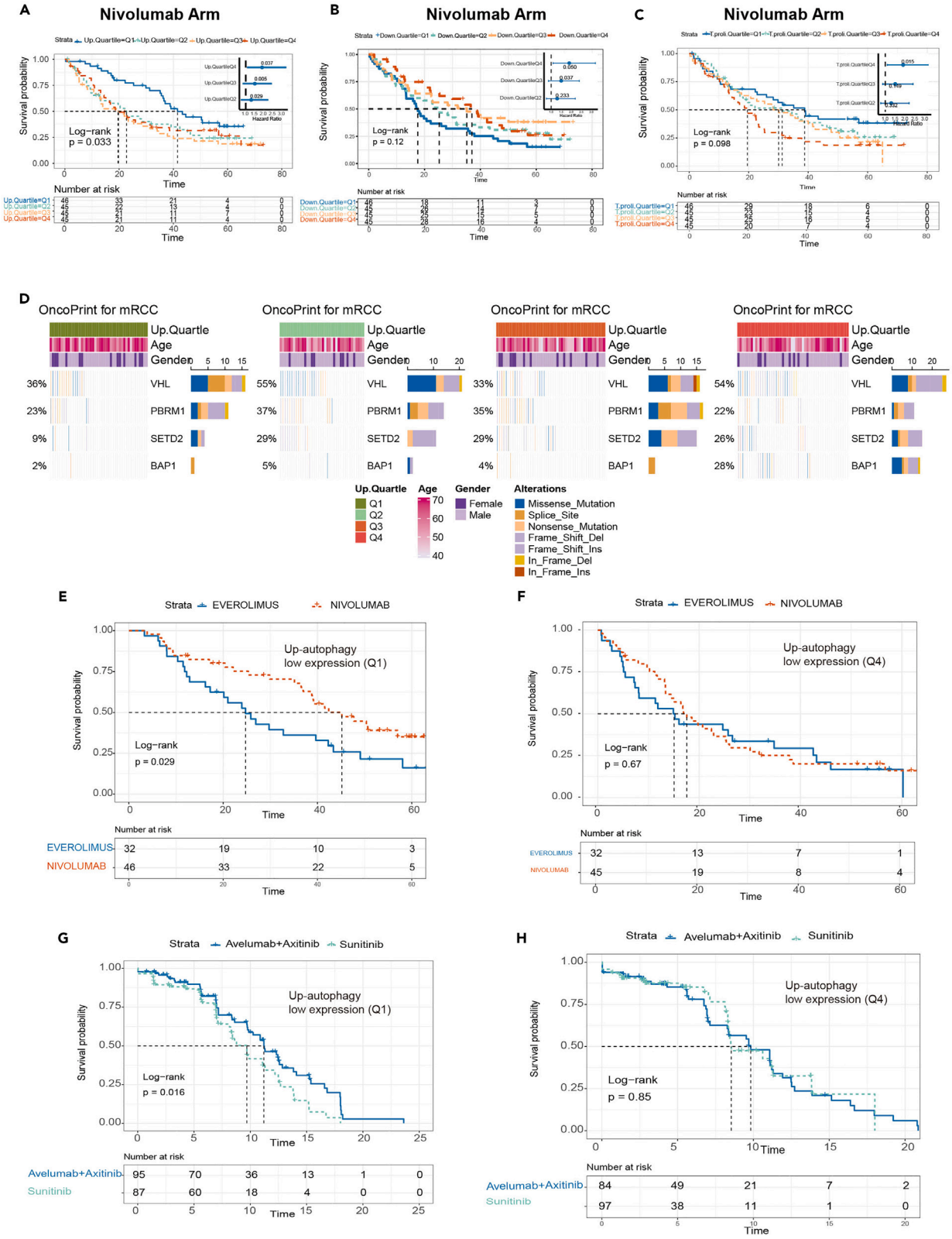
A
Nivolumab Arm
Log−rank
p = 0.033
Number at risk
B
Nivolumab Arm
Log−rank
p = 0.12
Number at risk
C
Nivolumab Arm
Log−rank
p = 0.098
Number at risk
D
OncoPrint for mRCC
Up.Quartle
Age
Gender
VHL
PBRM1
SETD2
BAP1
Up.Quartle
Q1
Q2
Q3
Q4
Age
Gender
Female
Male
Alterations
Missense_Mutation
Splice_Site
Nonsense_Mutation
Frame_Shift_Del
Frame_Shift_Ins
In_Frame_Del
In_Frame_Ins
E
Strata EVEROLIMUS NIVOLUMAB
Up-autophagy
low expression (Q1)
Log−rank
p = 0.029
Survival probability
Time
Number at risk
EVEROLIMUS 32 19 10 3
NIVOLUMAB 46 33 22 5
F
Strata EVEROLIMUS NIVOLUMAB
Up-autophagy
low expression (Q4)
Log−rank
p = 0.67
Survival probability
Time
Number at risk
EVEROLIMUS 32 13 7 1
NIVOLUMAB 45 19 8 4
G
Strata Avelumab+Axitinib Sunitinib
Up-autophagy
low expression (Q1)
Log−rank
p = 0.016
Survival probability
Time
Number at risk
Avelumab+Axitinib 95 70 36 13 1 0
Sunitinib 87 60 18 4 0 0
H
Strata Avelumab+Axitinib Sunitinib
Up-autophagy
low expression (Q4)
Log−rank
p = 0.85
Survival probability
Time
Number at risk
Avelumab+Axitinib 84 49 21 7 2
Sunitinib 97 38 11 1 0

Figure 6. Pan-cancer autophagy signature was associated with immunotherapeutic efficacy in the mRCC cohort

(A and B) Kaplan-Meier curves showing survival by the 1st-4th quartile (Q1-Q4) of up- and down-autophagy score in the mRCC patients who received anti-PD1 regimens.

(C) Kaplan-Meier curves showing survival by the 1st-4th quartile (Q1-Q4) score of the T proliferating cell score in the mRCC patients who received anti-PD1 regimens.

(D) Oncoprint showing gene mutation landscape stratified by 1st-4th quartile (Q1-Q4) of up-autophagy scores in the mRCC patients who received anti-PD1 regimens.

(E and F) The comparison of Kaplan-Meier curves depicting OS between anti-PD1 antibody and everolimus in the 1st quartile (Q1) and 4th quartile (Q4) of up-autophagy scores in the mRCC cohort.

(G and H) The comparison of Kaplan-Meier curves depicting PFS between anti-PD1 antibody and axitinib in the 1st quartile (Q1) and 4th quartile (Q4) of up-autophagy scores in the mRCC cohort.

observed significant correlations between up-autophagy scores and multiple metabolic components and metabolic regulation pathway (Table S9). Given that autophagy has important roles in regulating the interaction between different types of cells in the TME, which can shape the metabolic characteristics of the TME, enable immune escape of tumor cells, we further investigated the alterations of metabolic characteristics mediated by the autophagy signature.

We first applied ssGSEA using the metabolic related gene signatures including metabolic regulation pathway and metabolic core components to identify enrichment of gene sets correlated with the up- or down-autophagy scores using the transcriptomic and proteomics in the TCGA and CPTAC cohorts (Figures S10A and S10B). The enrichment of mRNA and protein levels highlighted similar modules that Myc, TNFα, glycolysis, hypoxia and cholesterol homeostasis signaling and oxidative phosphorylation, which were important regulators for tumor metabolic reported previously,[37–39] were significantly positively correlated with the up-autophagy score in the TCGA and CPTAC cohorts with transcriptomic and proteomics in multiple cancers (7 out of 8) (Figures S10A). While the down-autophagy signature played an inverse role in most pathways in multiple cancers (6 out of 8) (Figure S10B). Subsequently, pathway activations in metabolic core components including glycolysis, TCA cycle, metabolism of glucose glutamine and fatty acid were dramatically negatively or positively correlated with the up- or down-autophagy scores (Rho absolute value >0.2, FDR <0.05, Figures S10C–S10F).

Taken together, the pan-cancer autophagy signature may affect the metabolic features in various tumor cells, immune cells, and TME, thus regulating the interaction between different types of cells in the TME, altering tumor immunity as well as the efficacy of immunotherapy.

The validation of immunotherapeutic efficacy of autophagy signature with in-house cohort

To further validate the immunotherapeutic efficacy of autophagy signature, we retrospectively analyzed the patients who were diagnosed with advanced NSCLC, and received anti-PD(L)1 antibody regimen. The baseline characteristic was shown as Table S10. The ORR was 12.5%, and the median OS was 53 months. We observed the gradually increased survival from the bottom quartile (Q1) to the top quartile (Q4) of the up-autophagy scores (log rank for trend $p = 0.05$; Figure 8A), while the down-autophagy scores played the inverse role in predicting the immunotherapeutic efficacy (log rank for trend $p = 0.03$; Figure 8B). Further mechanism analysis observed the consistent signaling pathway activation as TCGA and CPTAC cohorts. We also evaluated the correlation between the autophagy score and T proliferating cells, the results showed that there is a positive and negative correlation with the up- and down-autophagy score (Up-autophagy: Rho = 0.39, $p < 0.01$; Down-autophagy: Rho = −0.26, $p < 0.01$; Figures S11A and S11B). Additionally, these important regulators for tumor metabolic including the TNFα, glycolysis, Myc, hypoxia,[37–39] were significantly positively correlated with the up-autophagy score in the in-house cohort (Figure 8C). While the down-autophagy signature played an inverse role in these pathways (Figure 8C). Congruently, the metabolic core components pathway was also consistent with the TCGA and CPTAC cohorts, that most pathway was positive with the down-autophagy score (Rho >0, FDR <0.05, Figure 8D; Table S11), while the up-autophagy score was not (Rho >0, FDR <0.05, Figure 8D; Table S11). This further supports the involvement of tumor metabolism in immune regulation mediated by the autophagy signature.

DISCUSSION

Specifically, we first manually curated list of autophagy-related genes according to previously published papers and public databases to classify the autophagy pathways. We then defined a pan-cancer autophagy signature by integrating the up- or downregulated autophagy genes, which were calculated by ssGSEA and applied across tissue types. Functional investigation further revealed a possible link between up-or down-autophagy signature and autophagy activation or inhibition. Subsequently, we demonstrated that the pan-cancer autophagy signature was not a property of tumor cells, but mainly derived from the T proliferating cells. Even so, the pan-cancer autophagy signature influenced the prognosis and immunotherapeutic efficacy independent of the T proliferating cell signature. Furthermore, the pan-cancer autophagy signature effected CCIs in the TME and could serve as a predictor for the immunotherapeutic outcome in multiple cancers. Our results suggested that these upregulated and downregulated gene signatures played inverse effects in terms of prognosis, immune prediction, and mechanism regulation, further strengthening the concept that integrative analysis of pathway-related genes without distinguishing activated or inhibitory was not appropriate.

Autophagy can be extensively induced in various cell types, but it has been shown to have context-dependent biological functions in different immune cells. The deletion of specific autophagy-related genes has been shown to induce several immunological alterations, including the differentiation of activated T cells into regulatory, memory or natural killer T cells.[32] In our study, the pan-cancer signature was prominently expressed in the T proliferating cells in multiple cancers, and it influenced the CCIs of immune cells. The tumors with

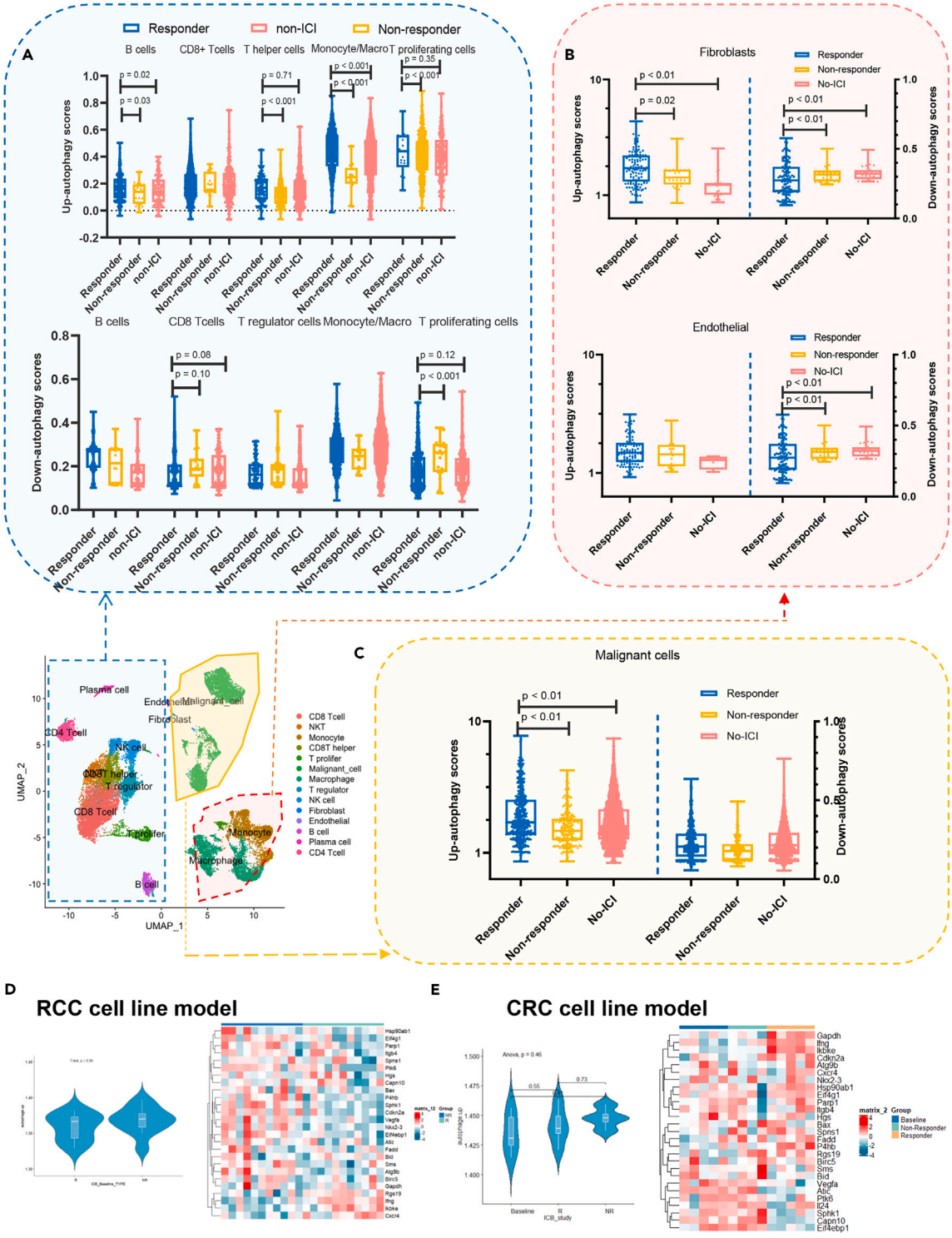

Figure 7. Immune cell but not cancer cell derived autophagy score contributed to the immune resistance

(A–C) The comparisons of up-autophagy scores and down-autophagy scores between untreated group and immune resistance group in the different immune cells, stromal cells, and the malignant cells. p values were compared by Mann-Whitney test. Data are represented as mean ± SEM.

(D) Heatmap depicting individual up-autophagy genes in the baseline, responders, or non-responders of anti-PD1 antibody in the mRCC cell line model.

(E) Heatmap depicting individual up-autophagy genes in the baseline, responders, or non-responders of anti-PD1 antibody in the CRC cell line model.

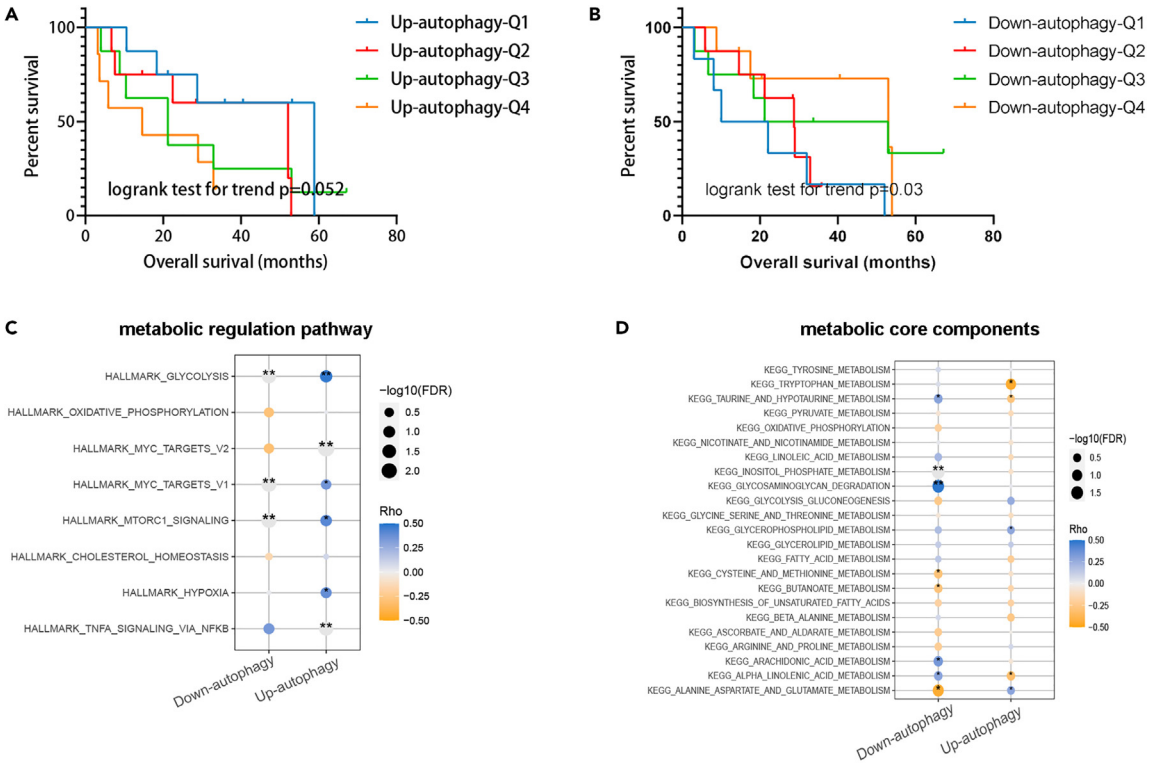

Figure 8. The validation of immunotherapeutic efficacy of autophagy signature with in-house cohort

(A and B) Unadjusted Kaplan-Meier curves showing survival by the quartile of the up-autophagy or down-autophagy score. p value was calculated by the log rank test (for trend).

(C) Bubble plot depicting the positive or negative correlations of up-autophagy scores or down-autophagy and metabolic regulation pathway (ssGSEA enrichment scores) in the in-house cohort (transcriptomics).

(D) Bubble plot depicting the positive or negative correlations of up-autophagy scores or down-autophagy and metabolic core components (ssGSEA enrichment scores) in the in-house cohort (transcriptomics).

high up-autophagy score (top 25% of quartile; Q4) significantly increased the CCIs between T proliferating cells and other immune cells, such as the T exhausted cells, T regulation cells, and monocyte/macrophages, but decreased the CCIs between T proliferating cells and T cytotoxic cells compared with the tumors with low up-autophagy score (bottom 25% of quartile; Q1), which may influence the efficacy of anti-PD1/anti-PDL1 regimen eventually, for which the tumor-killing effect was enhanced by reinvigorating the dysfunctional T cytotoxic cells.[40] Since the CCIs in the TME are of importance to the survival of multiple cancers,[30] autophagy most likely facilitates the immunosuppressive function of the T exhausted cells and T proliferating cells, thus influencing the prognosis and therapeutic efficacy.

As expected, subsequent analysis revealed that a high up-autophagy score was associated with inferior overall survival in mRCC patients who received anti-PD-1 treatment, while the down-autophagy score played an inverse predictive effect. The cancer cell-exogenous contribution of the up-autophagy signature to ICI resistance was further validated by excluding the contribution of cancer-specific cells, which was derived from the single-cell sequencing data[41] and the barcoded cell line model.[35] These results suggested that up-autophagy signature was involved in the T cell mediated anti-tumor immunity, providing insights into non-cell-autonomous effects of autophagy in the TME and potential influence on the immunotherapeutic efficacy eventually. Subsequently, we observed that the pan-cancer autophagy signature (integration of upregulated and downregulated genes) could play a role in predicting immunotherapeutic efficacy in mRCC, NSCLC, BLCA and melanoma cohorts. Moreover, the inverse role of up- or down autophagy score in the predicting the clinical outcomes was validated in an in-house cohort. Despite the potential of autophagy signature in predicting the efficacy of immunotherapy, prospective clinical trials with larger sample size were needed to validate the predictive efficacy.

Previously study seldom distinguished the cell-autonomous or non-cell-autonomous effects of gene signature in determining the fate of cancer cells base on bulk RNA sequencing, and the gene model or molecular subtypes based on the transcriptomic signature were susceptible to tumor purity, stromal context, or immune cell infiltration, making them less reproducible and robust in clinical practice. Although single-cell sequencing made it possible to distinguish the cell origins of specific gene signature, the high cost and big data handling limited its utility, especially in the context of the large clinical cancer cohorts.

Our research has identified a T proliferating cell-derived pan-autophagy signature that may influence the CCIs in the TME, thereby impacting the prognosis and efficacy of anti-PD-1/anti-PDL1 antibody. To do this, we conducted a comprehensive analysis using the TCGA cohort,

CPTAC cohort, multiple immunotherapeutic cohorts and scRNA-seq datasets including more than 10,000 patients. The immunotherapeutic efficacy was further validated in an in-house cohort. Our findings provide a line to identify the cell origin of gene signature in determining the fate of cancer cells and link pan-cancer gene signature to prognosis and immunotherapeutic efficacy, with potential for a variety of clinical applications including but not limited to (1) Pan-cancer lactate signature could serve as a predictor for ICIs regimen; (2) Combination therapeutic strategy such as autophagy blockade to overcome the primary immune resistance; (3) The potential to guide treatment choice-decision in the clinic for mRCC, although further validation with the perspective clinical trial is warranted; and (4) Pathway regulation target screening will help to identify more cancer-extrinsic resistant mechanisms.

This signature was able to map malignant cell states associated with ICI resistance, and it has both prognostic and predictive value that can be targeted therapeutically. Our study provides a path toward identifying therapeutic targets and combinations to combat treatment resistance.

Limitations of the study

There are also several limitations to be considered. First, although our statistical analysis showed that up-autophagy was predominantly expressed in T proliferating cells, it was not T proliferating cell specific, as these individual genes of pan-cancer autophagy signature were also expressed in other cells, such as macrophage cells, further study was warranted to exclude the cell-specific confounder factor. Second, the effect of pan-cancer autophagy on the CCIs in the TME was mainly based on in-silico approaches, and although the consistent results in multiple scRNA-seq datasets enhance the robustness, fundamental medical experiments are needed to definitively establish an interaction. Third, the mechanisms of up- and down autophagy signature need to be further investigated in the fundamental experiments. Lastly, biomarker-driven prospective clinical trials are needed to determine treatment-decision for advanced-stage tumors.

STAR★METHODS

Detailed methods are provided in the online version of this paper and include the following:

- KEY RESOURCES TABLE
- RESOURCE AVAILABILITY
  - Lead contact
  - Materials availability
  - Data and code availability
- EXPERIMENTAL MODEL AND STUDY PARTICIPANT DETAILS
  - Ethics approval and consent to participate
  - Patient cohort and sample collection
- METHOD DETAILS
  - The Cancer Genome Atlas (TCGA) cohort
  - Clinical proteomic tumor analysis consortium (CPTAC) cohort
  - Immunotherapy-related datasets
  - Cell–cell communication analysis
  - Barcoded CT26 mouse colorectal cancer cell line
  - RNA sequencing data of mouse renal cancer cell line (Renca) and mouse colorectal cancer cell line (CT26)
  - Single-cell RNA sequencing (scRNA-seq) datasets
- QUANTIFICATION AND STATISTICAL ANALYSIS

SUPPLEMENTAL INFORMATION

Supplemental information can be found online at https://doi.org/10.1016/j.isci.2023.108701.

ACKNOWLEDGMENTS

This study was supported by the National Natural Science Foundation of China (No. 81972726 and 82273074 for Yang T; 82241223 and U20A20360 for Lv GY), Dawn Project Foundation of Shanghai (No. 21SG36 for Yang T), and Shanghai Health Academic Leader Program (No. 2022XD001 for Yang T).

AUTHOR CONTRIBUTIONS

Conceptualization, G.L., T.Y., S.C., and C.L.; Methodology, Z.F., C.L., Y.J., N.W., and M.W.; Formal Analysis, Y.L., Z.F., C.L., Y.J., N.W., and M.W.; Investigation, Y.L., Z.F., C.L., Y.J., N.W., and M.W.; Resources, Y.L., C.L, Y.D., W.Q., X.Z., G.W., and S.C.; Data Curation, Y.L., S.F., C.L., C.W., and C.Z.; Writing, all authors; Visualization, Z.F., L.C., and Y.J.; Supervision, T.Y. and G.L; Funding Acquisition, T.Y. and G.L.

DECLARATION OF INTERESTS

C.L., X.Z., G.W., and S.C. are the employees of Burning Rock Biotech Inc. The other authors declare that they do not have any competing interests.

Received: May 25, 2023
Revised: September 11, 2023
Accepted: December 6, 2023
Published: December 8, 2023

REFERENCES

1. Xia, H., Green, D.R., and Zou, W. (2021). Autophagy in tumour immunity and therapy. Nat. Rev. Cancer *21*, 281–297.
2. Jiang, T., Chen, X., Ren, X., Yang, J.M., and Cheng, Y. (2021). Emerging role of autophagy in anti-tumor immunity: Implications for the modulation of immunotherapy resistance. Drug Resist. Updates *56*, 100752.
3. Jonge, M.M., Auguste, A., Wijk, M.V.L., Schouten, C.P., Meijers, M., Haar, T.T.N., Smit, V.T.H.B.M., A Nout, A.R., Glaire, A.M., Church, N.D., et al. (2019). Frequent Homologous Recombination Deficiency in High-Grade Endometrial Carcinomas. Clin Cancer Res. *25*, 1087–1097.
4. Yang, A., Herter-Sprie, G., Zhang, H., Lin, E.Y., Biancur, D., Wang, X., Deng, J., Hai, J., Yang, S., Wong, K.K., and Kimmelman, A.C. (2018). Autophagy Sustains Pancreatic Cancer Growth through Both Cell-Autonomous and Nonautonomous Mechanisms. Cancer Discov. *8*, 276–287.
5. Yamamoto, K., Venida, A., Yano, J., Biancur, D.E., Kakiuchi, M., Gupta, S., Sohn, A.S.W., Mukhopadhyay, S., Lin, E.Y., Parker, S.J., et al. (2020). Autophagy promotes immune evasion of pancreatic cancer by degrading MHC-I. Nature *581*, 100–105.
6. Clarke, A.J., and Simon, A.K. (2019). Autophagy in the renewal, differentiation and homeostasis of immune cells. Nat. Rev. Immunol. *19*, 170–183.
7. Homma, K., Suzuki, K., and Sugawara, H. (2011). The Autophagy Database: an all-inclusive information resource on autophagy that provides nourishment for research. Nucleic Acids Res. *39*, D986–D990.
8. Subramanian, A., Tamayo, P., Mootha, V.K., Mukherjee, S., Ebert, B.L., Gillette, M.A., Paulovich, A., Pomeroy, S.L., Golub, T.R., Lander, E.S., and Mesirov, J.P. (2005). Gene set enrichment analysis: a knowledge-based approach for interpreting genome-wide expression profiles. Proc. Natl. Acad. Sci. USA *102*, 15545–15550.
9. Luo, M., Ye, L., Chang, R., Ye, Y., Zhang, Z., Liu, C., Li, S., Jing, Y., Ruan, H., Zhang, G., et al. (2022). Multi-omics characterization of autophagy-related molecular features for therapeutic targeting of autophagy. Nat. Commun. *13*, 6345.
10. Levine, B., and Kroemer, G. (2019). Biological Functions of Autophagy Genes: A Disease Perspective. Cell *176*, 11–42.
11. Chakravarthy, A., Khan, L., Bensler, N.P., Bose, P., and De Carvalho, D.D. (2018). TGF-β-associated extracellular matrix genes link cancer-associated fibroblasts to immune evasion and immunotherapy failure. Nat. Commun. *9*, 4692.
12. Tuomisto, K., Palmu, J., Long, T., Watrous, J.D., Mercader, K., Lagerborg, K.A., Andres, A., Salmi, M., Jalkanen, S., Vasan, R.S., et al. (2022). A plasma metabolite score of three eicosanoids predicts incident type 2 diabetes: a prospective study in three independent cohorts. BMJ Open Diabetes Res. Care *10*, e002519.
13. Carter, S.L., Cibulskis, K., Helman, E., McKenna, A., Shen, H., Zack, T., Laird, P.W., Onofrio, R.C., Winckler, W., Weir, B.A., et al. (2012). Absolute quantification of somatic DNA alterations in human cancer. Nat. Biotechnol. *30*, 413–421.
14. Favero, F., Joshi, T., Marquard, A.M., Birkbak, N.J., Krzystanek, M., Li, Q., Szallasi, Z., and Eklund, A.C. (2015). Sequenza: allele-specific copy number and mutation profiles from tumor sequencing data. Ann. Oncol. *26*, 64–70.
15. Bao, L., Pu, M., and Messer, K. (2014). AbsCN-seq: a statistical method to estimate tumor purity, ploidy and absolute copy numbers from next-generation sequencing data. Bioinformatics *30*, 1056–1063.
16. Larson, N.B., and Fridley, B.L. (2013). PurBayes: estimating tumor cellularity and subclonality in next-generation sequencing data. Bioinformatics *29*, 1888–1889.
17. Newman, A.M., Liu, C.L., Green, M.R., Gentles, A.J., Feng, W., Xu, Y., Hoang, C.D., Diehn, M., and Alizadeh, A.A. (2015). Robust enumeration of cell subsets from tissue expression profiles. Nat. Methods *12*, 453–457.
18. Chakravarthy, A., Furness, A., Joshi, K., Ghorani, E., Ford, K., Ward, M.J., King, E.V., Lechner, M., Marafioti, T., Quezada, S.A., et al. (2018). Pan-cancer deconvolution of tumour composition using DNA methylation. Nat. Commun. *9*, 3220.
19. Cao, S., Wang, J.R., Ji, S., Yang, P., Dai, Y., Guo, S., Montierth, M.D., Shen, J.P., Zhao, X., Chen, J., et al. (2022). Estimation of tumor cell total mRNA expression in 15 cancer types predicts disease progression. Nat. Biotechnol. *40*, 1624–1633.
20. Li, T., Fu, J., Zeng, Z., Cohen, D., Li, J., Chen, Q., Li, B., and Liu, X.S. (2020). TIMER2. 0 for analysis of tumor-infiltrating immune cells. Nucleic Acids Res. *48*, W509–W514.
21. Rooney, M.S., Shukla, S.A., Wu, C.J., Getz, G., and Hacohen, N. (2015). Molecular and genetic properties of tumors associated with local immune cytolytic activity. Cell *160*, 48–61.
22. Kobayashi, H., Gieniec, K.A., Lannagan, T.R.M., Wang, T., Asai, N., Mizutani, Y., Iida, T., Ando, R., Thomas, E.M., Sakai, A., et al. (2022). The Origin and Contribution of Cancer-Associated Fibroblasts in Colorectal Carcinogenesis. Gastroenterology *162*, 890–906.
23. Puram, S.V., Tirosh, I., Parikh, A.S., Patel, A.P., Yizhak, K., Gillespie, S., Rodman, C., Luo, C.L., Mroz, E.A., Emerick, K.S., et al. (2017). Single-Cell Transcriptomic Analysis of Primary and Metastatic Tumor Ecosystems in Head and Neck Cancer. Cell *171*, 1611–1624.e24.
24. Song, Q., Hawkins, G.A., Wudel, L., Chou, P.C., Forbes, E., Pullikuth, A.K., Liu, L., Jin, G., Craddock, L., Topaloglu, U., et al. (2019). Dissecting intratumoral myeloid cell plasticity by single cell RNA-seq. Cancer Med. *8*, 3072–3085.
25. Ma, L., Hernandez, M.O., Zhao, Y., Mehta, M., Tran, B., Kelly, M., Rae, Z., Hernandez, J.M., Davis, J.L., Martin, S.P., et al. (2019). Tumor Cell Biodiversity Drives Microenvironmental Reprogramming in Liver Cancer. Cancer Cell *36*, 418–430.e6.
26. Zhang, P., Yang, M., Zhang, Y., Xiao, S., Lai, X., Tan, A., Du, S., and Li, S. (2019). Dissecting the Single-Cell Transcriptome Network Underlying Gastric Premalignant Lesions and Early Gastric Cancer. Cell Rep. *27*, 1934–1947.e5.
27. Bi, K., He, M.X., Bakouny, Z., Kanodia, A., Napolitano, S., Wu, J., Grimaldi, G., Braun, D.A., Cuoco, M.S., Mayorga, A., et al. (2021). Tumor and immune reprogramming during immunotherapy in advanced renal cell carcinoma. Cancer Cell *39*, 649–661.e5.
28. Sade-Feldman, M., Yizhak, K., Bjorgaard, S.L., Ray, J.P., de Boer, C.G., Jenkins, R.W., Lieb, D.J., Chen, J.H., Frederick, D.T., Barzily-Rokni, M., et al. (2018). Defining T Cell States Associated with Response to Checkpoint Immunotherapy in Melanoma. Cell *175*, 998–1013.e20.
29. Li, H., van der Leun, A.M., Yofe, I., Lubling, Y., Gelbard-Solodkin, D., van Akkooi, A.C.J., van den Braber, M., Rozeman, E.A., Haanen, J.B.A.G., Blank, C.U., et al. (2019). Dysfunctional CD8 T Cells Form a Proliferative, Dynamically Regulated Compartment within Human Melanoma. Cell *176*, 775–789.e18.
30. Armingol, E., Officer, A., Harismendy, O., and Lewis, N.E. (2021). Deciphering cell–cell interactions and communication from gene expression. Nat. Rev. Genet. *22*, 71–88.
31. Efremova, M., Vento-Tormo, M., Teichmann, S.A., and Vento-Tormo, R. (2020). CellPhoneDB: inferring cell-cell communication from combined expression of multi-subunit ligand-receptor complexes. Nat. Protoc. *15*, 1484–1506.
32. From the American Association of Neurological Surgeons AANS American Society of Neuroradiology ASNR Cardiovascular and Interventional Radiology Society of Europe CIRSE Canadian Interventional Radiology Association CIRA Congress of Neurological Surgeons CNS European Society of Minimally Invasive Neurological Therapy ESMINT European Society of Neuroradiology ESNR European Stroke Organization ESO Society for

Cardiovascular Angiography and Interventions SCAI Society of Interventional Radiology SIR Society of NeuroInterventional Surgery SNIS and World Stroke Organization WSO, Sacks, D., Baxter, B., Campbell, B.C.V., Carpenter, J.S., Cognard, C., Dippel, D., Eesa, M., Fischer, U., Hausegger, K., et al. (2018). Multisociety Consensus Quality Improvement Revised Consensus Statement for Endovascular Therapy of Acute Ischemic Stroke. Int. J. Stroke *13*, 612–632.

33. Braun, D.A., Hou, Y., Bakouny, Z., Ficial, M., Sant' Angelo, M., Forman, J., Ross-Macdonald, P., Berger, A.C., Jegede, O.A., Elagina, L., et al. (2020). Interplay of somatic alterations and immune infiltration modulates response to PD-1 blockade in advanced clear cell renal cell carcinoma. Nat. Med. *26*, 909–918.
34. Zemek, R.M., Chin, W.L., Fear, V.S., Wylie, B., Casey, T.H., Forbes, C., Tilsed, C.M., Boon, L., Guo, B.B., Bosco, A., et al. (2022). Temporally restricted activation of IFNβ signaling underlies response to immune checkpoint therapy in mice. Nat. Commun. *13*, 4895.
35. Gu, S.S., Wang, X., Hu, X., Jiang, P., Li, Z., Traugh, N., Bu, X., Tang, Q., Wang, C., Zeng, Z., et al. (2020). Clonal tracing reveals diverse patterns of response to immune checkpoint blockade. Genome Biol. *21*, 263.
36. Wei, S.C., Levine, J.H., Cogdill, A.P., Zhao, Y., Anang, N.A.A.S., Andrews, M.C., Sharma, P., Wang, J., Wargo, J.A., Pe'er, D., and Allison, J.P. (2017). Distinct Cellular Mechanisms Underlie Anti-CTLA-4 and Anti-PD-1 Checkpoint Blockade. Cell *170*, 1120–1133.e17.
37. Dey, P., Kimmelman, A.C., and DePinho, R.A. (2021). Metabolic Codependencies in the Tumor Microenvironment. Cancer Discov. *11*, 1067–1081.
38. Biswas, S.K. (2015). Metabolic Reprogramming of Immune Cells in Cancer Progression. Immunity *43*, 435–449.
39. Xia, L., Oyang, L., Lin, J., Tan, S., Han, Y., Wu, N., Yi, P., Tang, L., Pan, Q., Rao, S., et al. (2021). The cancer metabolic reprogramming and immune response. Mol. Cancer *20*, 28.
40. Kornepati, A.V.R., Vadlamudi, R.K., and Curiel, T.J. (2022). Programmed death ligand 1 signals in cancer cells. Nat. Rev. Cancer *22*, 174–189.
41. Jerby-Arnon, L., Shah, P., Cuoco, M.S., Rodman, C., Su, M.J., Melms, J.C., Leeson, R., Kanodia, A., Mei, S., Lin, J.R., et al. (2018). A Cancer Cell Program Promotes T Cell Exclusion and Resistance to Checkpoint Blockade. Cell *175*, 984–997.e24.
42. Hugo, W., Zaretsky, J.M., Sun, L., Song, C., Moreno, B.H., Hu-Lieskovan, S., Berent-Maoz, B., Pang, J., Chmielowski, B., Cherry, G., et al. (2016). Genomic and Transcriptomic Features of Response to Anti-PD-1 Therapy in Metastatic Melanoma. Cell *165*, 35–44.
43. Liu, D., Schilling, B., Liu, D., Sucker, A., Livingstone, E., Jerby-Arnon, L., Zimmer, L., Gutzmer, R., Satzger, I., Loquai, C., et al. (2019). Integrative molecular and clinical modeling of clinical outcomes to PD1 blockade in patients with metastatic melanoma. Nat. Med. *25*, 1916–1927.
44. Riaz, N., Havel, J.J., Makarov, V., Desrichard, A., Urba, W.J., Sims, J.S., Hodi, F.S., Martín-Algarra, S., Mandal, R., Sharfman, W.H., et al. (2017). Tumor and Microenvironment Evolution during Immunotherapy with Nivolumab. Cell *171*, 934–949.e16.
45. Ravi, A., Hellmann, M.D., Arniella, M.B., Holton, M., Freeman, S.S., Naranbhai, V., Stewart, C., Leshchiner, I., Kim, J., Akiyama, Y., et al. (2023). Genomic and transcriptomic analysis of checkpoint blockade response in advanced non-small cell lung cancer. Nat. Genet. *55*, 807–819.
46. Borcherding, N., Vishwakarma, A., Voigt, A.P., Bellizzi, A., Kaplan, J., Nepple, K., Salem, A.K., Jenkins, R.W., Zakharia, Y., and Zhang, W. (2021). Mapping the immune environment in clear cell renal carcinoma by single-cell genomics. Commun. Biol. *4*, 122.
47. Wu, T.D., Madireddi, S., de Almeida, P.E., Banchereau, R., Chen, Y.J.J., Chitre, A.S., Chiang, E.Y., Iftikhar, H., O'Gorman, W.E., Au-Yeung, A., et al. (2020). Peripheral T cell expansion predicts tumour infiltration and clinical response. Nature *579*, 274–278.
48. Zhang, M., Yang, H., Wan, L., Wang, Z., Wang, H., Ge, C., Liu, Y., Hao, Y., Zhang, D., Shi, G., et al. (2020). Single-cell transcriptomic architecture and intercellular crosstalk of human intrahepatic cholangiocarcinoma. J. Hepatol. *73*, 1118–1130.
49. Team RC (2013). R: A Language and Environment for Statistical Computing.
50. Allaire, J. (2012). RStudio: integrated development environment for R *770* (394), 165–171.
51. Ritchie, M.E., Phipson, B., Wu, D., Hu, Y., Law, C.W., Shi, W., and Smyth, G.K. (2015). limma powers differential expression analyses for RNA-sequencing and microarray studies. Nucleic Acids Res. *43*, e47.
52. Wu, T., Hu, E., Xu, S., Chen, M., Guo, P., Dai, Z., Feng, T., Zhou, L., Tang, W., Zhan, L., et al. (2021). clusterProfiler 4.0: A universal enrichment tool for interpreting omics data. Innovation *2*, 100141.
53. Gu, Z., Eils, R., and Schlesner, M. (2016). Complex heatmaps reveal patterns and correlations in multidimensional genomic data. Bioinformatics *32*, 2847–2849.
54. Hänzelmann, S., Castelo, R., and Guinney, J. (2013). GSVA: gene set variation analysis for microarray and RNA-seq data. BMC Bioinf. *14*, 7.
55. Yu, G., Wang, L.G., Han, Y., and He, Q.Y. (2012). clusterProfiler: an R package for comparing biological themes among gene clusters. OMICS *16*, 284–287.
56. Gaujoux, R., and Seoighe, C. (2010). A flexible R package for nonnegative matrix factorization. BMC Bioinf. *11*, 367.
57. Lin, H., and Zelterman, D. (2002). Modeling Survival Data: Extending the Cox Model (Taylor & Francis).
58. Kassambara, A., Kosinski, M., and Biecek, P. (2019). Survminer: survival analysis and visualization. R package version 04 *7*.
59. Carlson, M., Falcon, S., Pages, H., and Li, N. (2019). org. Hs. eg. db: Genome wide annotation for Human. R package version *3*, 3.
60. Hao, Y., Hao, S., Andersen-Nissen, E., Mauck, W.M., III, Zheng, S., Butler, A., Lee, M.J., Wilk, A.J., Darby, C., Zager, M., et al. (2021). Integrated analysis of multimodal single-cell data. Cell *184*, 3573–3587.
61. Szolek, A., Schubert, B., Mohr, C., Sturm, M., Feldhahn, M., and Kohlbacher, O. (2014). OptiType: precision HLA typing from next-generation sequencing data. Bioinformatics *30*, 3310–3316.
62. Belkina, C.A., Ciccolella, O.C., Halpert, R., Spidlen, J., and Snyder-Cappione, E.J. (2019). Nat Commun *10*, 5415.
63. Sievert, C., Parmer, C., Hocking, T., Chamberlain, S., Ram, K., Corvellec, M.,Despouy P. & Brüggemann ,S. (2021). Package 'plotly'. *R Foundation for Statistical Computing*, Vienna. https://cran.r-project.org/package=plotly.
64. Kuhn, M. (2015). Caret: Classification and Regression Training (Astrophysics Source Code Library).
65. Kuilman, T., Velds, A., Kemper, K., Ranzani, M., Bombardelli, L., Hoogstraat, M., Nevedomskaya, E., Xu, G., de Ruiter, J., Lolkema, M.P., et al. (2015). CopywriteR: DNA copy number detection from off-target sequence data. Genome Biol. *16*, 49.
66. Kassambara, A., and Kassambara, M.A. (2019). Package 'ggcorrplot. R package version 01 *3*.
67. McInnes, L., Healy, J., and Melville, J. (2018). Umap: Uniform manifold approximation and projection for dimension reduction. Preprint at. arXiv, 10. https://doi.org/10.48550/arXiv.1802.03426.
68. Schubert, M., Klinger, B., Klünemann, M., Sieber, A., Uhlitz, F., Sauer, S., Uhlitz, F., Sauer, S., and Garnett, J.M. (2018). Blüthgen N.,et al. Perturbation-response genes reveal signaling footprints in cancer gene expression. Nat. Commun. *9*, 1–11.
69. Jin, S., Guerrero-Juarez, C.F., Zhang, L., Chang, I., Ramos, R., Kuan, C.H., Myung, P., Plikus, M.V., and Nie, Q. (2021). Inference and analysis of cell-cell communication using CellChat. Nat. Commun. *12*, 1088.
70. Owens, N.D., De Domenico, E., and Gilchrist, M.J. (2019). An RNA-Seq Protocol for Differential Expression Analysis. Cold Spring Harb. Protoc. *2019*, pdb.prot098368.
71. ICGC/TCGA Pan-Cancer Analysis of Whole Genomes Consortium (2020). Pan-cancer analysis of whole genomes. Nature *578*, 82–93.
72. Law, C.W., Chen, Y., Shi, W., and Smyth, G.K. (2014). voom: Precision weights unlock linear model analysis tools for RNA-seq read counts. Genome Biol. *15*, R29.
73. de Jonge, M.M., Auguste, A., van Wijk, L.M., Schouten, P.C., Meijers, M., Ter Haar, N.T., Smit, V.T.H.B.M., Nout, R.A., Glaire, M.A., Church, D.N., et al. (2019). Frequent Homologous Recombination Deficiency in High-grade Endometrial Carcinomas. Clin. Cancer Res. *25*, 1087–1097.
74. Yoshihara, K., Shahmoradgoli, M., Martínez, E., Vegesna, R., Kim, H., Torres-Garcia, W., Treviño, V., Shen, H., Laird, P.W., Levine, D.A., et al. (2013). Inferring tumour purity and stromal and immune cell admixture from expression data. Nat. Commun. *4*, 2612.
75. Vasaikar, S., Huang, C., Wang, X., Petyuk, V.A., Savage, S.R., Wen, B., Dou, Y., Zhang, Y., Shi, Z., Arshad, O.A., et al. (2019). Proteogenomic Analysis of Human Colon Cancer Reveals New Therapeutic Opportunities. Cell *177*, 1035–1049.e19.
76. Dou, Y., Kawaler, E.A., Cui Zhou, D., Gritsenko, M.A., Huang, C., Blumenberg, L., Karpova, A., Petyuk, V.A., Savage, S.R., Satpathy, S., et al. (2020). Proteogenomic Characterization of Endometrial Carcinoma. Cell *180*, 729–748.e26.
77. Wang, L.B., Karpova, A., Gritsenko, M.A., Kyle, J.E., Cao, S., Li, Y., Rykunov, D., Colaprico, A., Rothstein, J.H., Hong, R., et al. (2021). Proteogenomic and metabolomic characterization of human glioblastoma. Cancer Cell *39*, 509–528.e20.
78. Zhang, Y., Chen, F., Chandrashekar, D.S., Varambally, S., and Creighton, C.J. (2022). Proteogenomic characterization of 2002 human cancers reveals pan-cancer molecular

subtypes and associated pathways. Nat. Commun. *13*, 2669.

79. Motzer, R.J., Robbins, P.B., Powles, T., Albiges, L., Haanen, J.B., Larkin, J., Mu, X.J., Ching, K.A., Uemura, M., Pal, S.K., et al. (2020). Avelumab plus axitinib versus sunitinib in advanced renal cell carcinoma: biomarker analysis of the phase 3 JAVELIN Renal 101 trial. Nat. Med. *26*, 1733–1741.
80. Choueiri, T.K., Fishman, M.N., Escudier, B., McDermott, D.F., Drake, C.G., Kluger, H., Stadler, W.M., Perez-Gracia, J.L., McNeel, D.G., Curti, B., et al. (2016). Immunomodulatory Activity of Nivolumab in Metastatic Renal Cell CarcinomaImmunomodulatory Activity of Nivolumab in mRCC. Clin. Cancer Res. *22*, 5461–5471.
81. Motzer, R.J., Rini, B.I., McDermott, D.F., Redman, B.G., Kuzel, T.M., Harrison, M.R., Vaishampayan, U.N., Drabkin, H.A., George, S., Logan, T.F., et al. (2015). Nivolumab for Metastatic Renal Cell Carcinoma: Results of a Randomized Phase II Trial. J. Clin. Oncol. *33*, 1430–1437.
82. Motzer, R.J., Tannir, N.M., McDermott, D.F., Arén Frontera, O., Melichar, B., Choueiri, T.K., Plimack, E.R., Barthélémy, P., Porta, C., George, S., et al. (2018). Nivolumab plus Ipilimumab versus Sunitinib in Advanced Renal-Cell Carcinoma. N. Engl. J. Med. *378*, 1277–1290.
83. Bhang, H.e.C., Ruddy, D.A., Krishnamurthy Radhakrishna, V., Caushi, J.X., Zhao, R., Hims, M.M., Singh, A.P., Kao, I., Rakiec, D., Shaw, P., et al. (2015). Studying clonal dynamics in response to cancer therapy using high-complexity barcoding. Nat. Med. *21*, 440–448.
84. Van Allen, E.M., Miao, D., Schilling, B., Shukla, S.A., Blank, C., Zimmer, L., Sucker, A., Hillen, U., Foppen, M.H.G., Goldinger, S.M., et al. (2015). Genomic correlates of response to CTLA-4 blockade in metastatic melanoma. Science *350*, 207–211.
85. Snyder, A., Makarov, V., Merghoub, T., Yuan, J., Zaretsky, J.M., Desrichard, A., Walsh, L.A., Postow, M.A., Wong, P., Ho, T.S., et al. (2014). Genetic basis for clinical response to CTLA-4 blockade in melanoma. N. Engl. J. Med. *371*, 2189–2199.
86. Shih, A.J., Menzin, A., Whyte, J., Lovecchio, J., Liew, A., Khalili, H., Bhuiya, T., Gregersen, P.K., and Lee, A.T. (2018). Identification of grade and origin specific cell populations in serous epithelial ovarian cancer by single cell RNA-seq. PLoS One *13*, e0206785.
87. Sun, D., Wang, J., Han, Y., Dong, X., Ge, J., Zheng, R., Shi, X., Wang, B., Li, Z., Ren, P., et al. (2021). TISCH: a comprehensive web resource enabling interactive single-cell transcriptome visualization of tumor microenvironment. Nucleic Acids Res. *49*, D1420–D1430.
88. Chen, B., Khodadoust, M.S., Liu, C.L., Newman, A.M., and Alizadeh, A.A. (2018). Profiling Tumor Infiltrating Immune Cells with CIBERSORT. Methods Mol. Biol. *1711*, 243–259.

STAR★METHODS

KEY RESOURCES TABLE

REAGENT or RESOURCE	SOURCE	IDENTIFIER
Deposited data		
In-house mRNA data	In this paper	with accession No. Project IDOEP004524 (https://www.biosino.org/bmdc/database/ngdcResource)
Pan-cancer samples (15 types of cancer)	USCS XENA portal	TCGA (https://portal.gdc.cancer.gov/); USCS XENA portal (https://xena.ucsc.edu/)
Pan-cancer samples (10 types of cancer)	The omics database	CPTCA (https://proteomics.cancer.gov/programs/cptac); The omics database (http://www.linkedomics.org/login.php)
Anti-PD-1-treated melanoma-Hugo	Hugo et al.[42]	GEO: GSE78220, GEO: GSE96619
Anti-PD-1-treated metastatic melanoma-Liu	Liu et al.[43]	dbGaP: phs000452
Anti-PD-1-treated advanced melanoma-Riaz	Riaz et al.[44]	GEO: GSE91061
Anti-PD-1-treated metastatic clear cell renal cell carcinoma	Braun et al.[33]	Supplementary Table
Anti-PD-L1-treated bladder cancer	IMvigor210CoreBiologies	EGA: EGAS00001002556 (http://research-pub.gene.com/IMvigor210CoreBiologies)
Anti-PD-1-treated non-small cell lung cancer	Ravi et al.[45]	Supplementary Table
Kidney Renal Clear Cell Carcinoma (KIRC) scRNA-seq dataset	Borcherding et al.[46]	GEO: GSE121636 (http://tisch.comp-genomics.org/search-gene/)
Kidney Renal Clear Cell Carcinoma (KIRC) scRNA-seq dataset	Wu et al.[47]	GEO: GSE139555 (http://tisch.comp-genomics.org/search-gene/)
Cholangiocarcinoma (CHOL) scRNA-seq dataset	Zhang et al.[48]	GEO: GSE138709 (http://tisch.comp-genomics.org/search-gene/)
(CRC) scRNA-seq dataset	Zhang et al.[26]	GEO: GSE134520 (http://tisch.comp-genomics.org/search-gene/)
mRCC scRNA-seq dataset	Biet al.[27]	Supplementary Table
Barcoded CT26 mouse colorectal cancer cell line	(TISMO) database	GEO: GSE1394767 (TISMO) database (http://tismo.cistrome.org/)
Mouse renal cancer cell line (Renca)	(TISMO) database	GEO: GSE153941 (TISMO) database (http://tismo.cistrome.org/)
Software and algorithms		
R (version 4.1.2)	Team et al.[49]	https://www.r-project.org/
R studio	Allaire et al.[50]	https://www.rstudio.com/products/rstudio/
Limma R package (version 3.52.2)	Ritchie et al.[51]	https://bioconductor.org/packages/release/bioc/html/limma.html
clusterProfiler R package (version 4.4.4)	Wu et al.[52]	https://www.bioconductor.org/packages/release/bioc/html/clusterProfiler.html
ComplexHeatmap R package (version 2.12.1)	Gu et al.[53]	http://www.bioconductor.org/packages/release/bioc/html/ComplexHeatmap.html
GSVA (version 1.44.5)	Hanzelmann et al.[54]	http://www.bioconductor.org/packages/release/bioc/html/GSVA.html
NMF R package (version 0.24.0)	Yu et al.[55,56]	https://cran.r-project.org/web/packages/NMF/index.html
survival R package (version 3.4.0)	Lin et al.[57]	https://cran.r-project.org/web/packages/survival/index.html

(*Continued on next page*)

Continued

REAGENT or RESOURCE	SOURCE	IDENTIFIER
survminer R package (version 0.4.9)	Kassambara et al.[58]	https://cran.r-project.org/web/packages/survminer/index.html
org.Hs.e.g.,.db R package (version 3.15.0)	Carlson et al.[59]	https://bioconductor.org/packages/release/data/annotation/html/org.Hs.e.g.,.db.html
Seurat (version 4.0)	Hao et al.[60]	https://satijalab.org/seurat/
tSNE (version 0.1–3.1)	Donaldson et al.[61,62]	https://cran.r-project.org/web/packages/tsne/index.html
plotly (version 4.0)	Plotly et al.[63]	https://plotly.com/r/
caret R package (version 6.0–93)	Kuhn et al.[64]	https://cran.r-project.org/web/packages/caret/index.html
MethylCIBERSORT (version 0.2.0)	Chakravarthy et al.[18]	https://zenodo.org/record/1284582#.YzajM3ZBy3A
ggcorrplot R package (version 0.1.4)	Kassambara et al.[65,66]	https://cloud.r-project.org/web/packages/ggcorrplot/
UMAP R package (version 0.2.9.0)	McInnes et al.[67]	https://bioconductor.org/packages/release/bioc/html/MutationalPatterns.html
PROGENy (version1.18.0)	Schubert et al.[68]	https://saezlab.github.io/progeny/
ComplexHeatmap R package (version 0.2.9.0)	Gu et al.[53]	https://bioconductor.org/packages/release/bioc/html/ComplexHeatmap.html
CellChat (v1.1.2)	Jin et al.[69]	https://github.com/sqjin/CellChat
GraphPad Prism version 9	(GraphPad Software, La Jolla, CA)	https://www.graphpad.com/

RESOURCE AVAILABILITY

Lead contact

This study did not generate new unique reagents. Further information and requests for resources and regents should be directed to and will be fulfilled by the lead author, Guoyue Lv, e-mail: lvgy@jlu.edu.cn.

Materials availability

This study did not generate new unique reagents.

Data and code availability

All the data in the current study are available from the public datasets listed in the key resources table.

The code used in this study are available on reasonable request.

Any additional information required to reanalyze the data reported in this paper is available from the lead contact upon request.

EXPERIMENTAL MODEL AND STUDY PARTICIPANT DETAILS

Ethics approval and consent to participate

This study was approved by the ethics committees of the Cancer Hospital, Chinese Academy of Medical Sciences, and conducted in accordance with the Declaration of Helsinki and the international standards of good clinical practice. The median follow-up time was 53 months. All patients have informed consent, and this study was approved by the ethics committees of the National Cancer Center (No.17-202/1458).

Patient cohort and sample collection

Totally, tissue samples from 32 advanced-stage NSCLC patients who treated with anti-PD-(L)1 antibodies at National Cancer Center/Cancer Hospital and Chinese Academy of Medical Sciences from April 2017 to September 2018 were retrospectively analyzed. Eligibility criteria included being aged 18 to 75 years; having an Eastern Cooperative Oncology Group score of 0 or 1; having histologically confirmed and standard treatment–recurrent or standard treatment–intolerant stage IV NSCLC; RNA extraction, sequencing library construction, sequencing and FASTQ data quality control were performed in accordance with the protocol by Nick D.L. Owens et al.[70]

METHOD DETAILS

The Cancer Genome Atlas (TCGA) cohort

Overall, 15 types of solid tumors (carcinomas) with normal tumors more than 10 in the TCGA cohort were used in this study (Table S1). These included bladder urothelial carcinoma (BLCA), breast invasive carcinoma (BRCA), colon adenocarcinoma (COAD), rectum adenocarcinoma

(READ), esophageal carcinoma (ESCA), stomach adenocarcinoma (STAD), kidney chromophobe (KICH), kidney renal clear cell carcinoma (KIRC), kidney renal papillary cell carcinoma (KIRP), liver hepatocellular carcinoma (LIHC), lung adenocarcinoma (LUAD), lung squamous cell carcinoma (LUSC), head and neck squamous cell carcinoma (HNSCC), pancreatic adenocarcinoma (PAAD), thyroid carcinoma (THCA), and uterine corpus endometrial carcinoma (UCEC). COAD and READ were combined into colorectal adenocarcinomas (COREAD) (Cancer Genome Atlas Network, 2022). Transcriptomic data was downloaded from the USCS XENA portal (https://xena.ucsc.edu/) as log2 (TPM+0.001), and clinical and mutation data were downloaded from the GDC TCGA data portal (MC3 dataset).[71] Patients with missing clinical annotation were removed, resulting in a total of 6,431 samples (Table S1).

Limma-trend[11,72] was used to identify differentially expressed genes (DEGs) between normal and cancer samples while controlling for cancer type at a false discovery rate (FDR) < 0.05 and 0.5-fold-change. This was done to minimize the effects of class imbalance and to derive a picture of autophagy pathway genes dysregulation independent of cancer type.

The significant up-regulated and down-regulated autophagy pathway-related genes were used to define up-autophagy score and down-autophagy score by using the R package "GSVA".[54] Up-autophagy scores and down-autophagy scores were divided into quartiles for categorization. A stratified Cox regression model was used to estimate prognostication, and the formula was Survival ~ up-autophagy-quartile + down-autophagy-quartile + strata (cancer type) + strata(stage).

The purity of the tumor cells was estimated using ABSOLUTE,[13] AbsCN-seq,[15] ASCAT,[14] PurBayes,[16] CPE,[73] ESTIMATE,[74] as previously described. The tumour-specific total mRNA expression (TmS) was obtained from a previous study.[19] Spearman's correlation was used to determine the correlation between the up-autophagy score or down-autophagy score and TmS.

The MC3 MAF (Synapse: syn7214402) was used to obtain the median variant allele frequency (VAF) of mutations. To estimate cellular fractions, MethylCIBERSORT[18] was employed and Spearman's rank correlations between the up- and down-scores of autophagy were determined during cellular deconvolution analyses. To identify potential neoantigens and variants, Topiary (https://github.com/openvax/topiary) was utilized in conjunction with the MC3 set of TCGA mutation calls (Synapse: syn7214402) using monomers and a binding affinity threshold of <500 nM. Additionally, the mutation loads were calculated for the same set of samples.

Clinical proteomic tumor analysis consortium (CPTAC) cohort

Proteomic datasets

We obtained the CPTAC dataset of mass spectrometry-based proteomics data from 10 cancer types from the omics database (http://www.linkedomics.org/login.php). The cancer types included BRCA, COAD, Glioblastoma (GBM)), HNSCC, LUAD, LUSC, Ovarian Serous Cystadenocarcinoma, PAAD, Prostate Adenocarcinoma (PRAD), and UCEC.[75–78] The above studies analyzed the tumors using global proteomic profiling by liquid chromatography-tandem mass spectrometry (LC-MS/MS). Proteomic data, as provided by the CPTAC Data Portal and related publications, were processed, and normalized as previously.[79] The proteomic data in the CPTAC was used to evaluate the correlation between up-or down-autophagy scores and autophagy related protein, including lapidate microtubule-associated protein 1A/1B-light chain 3A (LC3A) and LC3B expression.

Transcriptomic datasets

We then obtained 1,072 human tumors with proteomics data and corresponding RNA-seq data from the Broad Institute's Firehose data portal (https://gdac.broadinstitute.org) and the Genome Data Commons [https://gdc.cancer.gov/]. Expression values were normalized across samples to standard deviations from the median within each cancer type and dataset. The R package "GSVA"[54] was used to calculate the up-autophagy and down-autophagy scores.

Immunotherapy-related datasets

Metastatic renal cell carcinoma (mRCC) cohort

The clinical characteristics and survival of two metastatic clear cell renal cell carcinoma (mRCC) immunotherapeutic datasets were extracted from two previous study.[33,80] For CheckMate study,[33] data from prospective clinical trials of the anti-PD-1 antibody nivolumab in mRCC were included.[56,81,82] The mRNA expression was united as log2 (TPM+0.001) and the $CD8^+$ T cells counts and density in the tumor margin and tumor central were measured by a multiplex immunofluorescence assay.[3] For JAVELIN Renal 101 trial,[80] the mRNA expression was derived from previous study.[80] To conduct further analysis of individual genes or standardized gene pathway signature scores, the TPM values underwent either log2 transformation or standardization. Up-autophagy and down-autophagy scores were calculated using single sample gene set enrichment analysis (ssGSEA) with the R package "GSVA". The correlations between up-autophagy or down-autophagy scores and different infiltrated immune cells were calculated by Spearman's correlation. Non-negative matrix factorization (NMF) clustering was performed by the R package "NMF".[45]

NSCLC cohort

The clinical characteristics and survival of the NSCLC immunotherapeutic cohort (SU2C-MARK) were extracted from the published study.[83] Data were retrospective analyzed from clinical trials of the anti-PD(L)-1 antibody. The samples with monotherapy (single agent anti-PD-1/anti-PDL1 antibody) were analyzed. The log2-transromed TPMs of RNA-seq data were download from the supplementary material,[83] and genes with low expression (expression value was 0 in more than 50% samples) were removed from subsequently analysis. Up-autophagy

and down-autophagy scores were calculated using single sample gene set enrichment analysis (ssGSEA) with the R package "GSVA". NMF clustering were performed by the R package "NMF".[45]

Bladder (BLCA) cohort

The pre-treatment tumor samples from a large phase 2 trial (IMvigor210) of bladder cancer were used to evaluate the clinical efficacy of PD-L1 blockade with atezolizumab in mUC (http://research-pub.gene.com/IMvigor210CoreBiologies). Up-autophagy and down-autophagy scores were calculated using single sample gene set enrichment analysis (ssGSEA) with the R package "GSVA". The correlations between up-autophagy or down-autophagy scores and different infiltrated immune cells were calculated by Spearman's correlation. NMF clustering were performed by the R package "NMF".[45]

Melanoma datasets

In our study, transcriptomics sequencing data and survival data from two melanoma datasets containing patients who received anti-PD-1 antibodies[42–44,84,85] were analyzed. For the Liu cohort,[85] patients who were treated or ever treated combined with Ipilimumab (IPI) were excluded from analysis. Up autophagy and down autophagy score were calculated by ssGSEA using the R package "GSVA". NMF clustering were performed by the R package "NMF".[45]

Cell–cell communication analysis

CellChat (v1.1.2)[69] was used to identify and visualize cell-cell interactions between different cell types. The "createCellChat" function was used to create a CellChat object from Seurat normalized data, and the "addMeta" and "setIdent" functions was applied to add clusters labeled in the previous Seurat object. The "identifyOverExpressedGenes", "identifyOverExpressedInteractions" functions was utilized to identify over-expressed ligands or receptors based on the CellChat human database. The "computeCommunProb" and "filterCommunication" functions (min. cells = 10) computed communication probability and inferred cellular communication network. The "computeCommunProbPathway" and "aggregateNet" functions were ran to infer the cell-cell communication at a signaling pathway level between each cluster.

Barcoded CT26 mouse colorectal cancer cell line

To assess the role of the cancer intrinsic up-autophagy signature in the ICI resistance at the cellular level, we employed the previously published mouse CT26 colorectal cancer cell line model,[35] which utilized the ClonTracer barcoding system[54] to uniquely label clones in CT26 cell populations for *in vivo* study. The recipient mice were transplanted with the barcoded cells and treated with control IgG, anti-PD-1. The responders or non-responders of ICI treatment were determined by the tumor volume alterations after anti-PD-1 treatment compared with the control IgG-administrated mice, as previous reported.[35]

RNA sequencing data of mouse renal cancer cell line (Renca) and mouse colorectal cancer cell line (CT26)

The GEO accession number GSE153941 and GSE1394767 contains the raw sequencing data of the mouse renal cancer cell line (Renca)[34] and mouse colorectal cancer cell line (CT26).[35] The processed and normalized data was obtained from the Tumor Immune Syngeneic MOuse (TISMO) database (http://tismo.cistrome.org/). The transcriptomic data was presented as log2 (TPM+0.001) and was standardized by quantile normalization. Up autophagy scores were calculated by ssGSEA using the R package "GSVA".[86]

Single-cell RNA sequencing (scRNA-seq) datasets

Multiple types of cancers including RCC (GSE121636),[24] KIRC (GSE139555),[25] CHOL(GSE138709),[25] CRC (GSE134520)[87] were download from the Tumor Immune Single-cell Hub (TISCH) (http://tisch.comp-genomics.org/search-gene/), a scRNA-seq database focusing on TME. TISCH provides detailed cell-type annotation at the single-cell level (malignant cells, stomal cells and immune cells type), enabling the exploration of TME across different cancer types. The standardized analysis workflow for processing all the collected datasets, including quality control, batch effect removal, cell clustering, differential expression analysis, cell-type annotation, malignant cell classification and gene set enrichment analysis, was described in a previous study.[88] The up autophagy and down autophagy signature were determined as the geometric means of the associated gene transcript levels (0.01 offset). The differences of up autophagy or down signatures across different cell types were measured by Kruskal-Wallis's test.

The processed sRNA-seq data from mRCC dataset (GSE103322, anti-PD-L1 combined with anti-CTLA4 antibody, n = 25) was derived from previous study.[23,41] Quality control, batch effect removal, cell clustering, differential expression analysis, cell-type annotation, malignant cell classification was described previously.[23] The cell type was re-annotated according to the established cell type specific markers (Table S2), and single R package and previous original papers. Additionally, the up-autophagy and down-autophagy scores of immune resistant and immune untreated patients were compared in malignant cells, immune cells, and stromal cells.

QUANTIFICATION AND STATISTICAL ANALYSIS

Statistical analyses were conducted with GraphPad Prism version 9 (GraphPad Software, La Jolla, CA) or R versions 4.1.2. Spearman's correlation analysis was performed using the R package *stats* version 4.1.2. Continuous data were compared between two groups using the

Wilcoxon test, and between multiple groups using the Kruskal-Wallis's test. Categorical data were compared between two groups using Fisher's exact test. Wilcoxon's rank-sum test was performed to calculate the cell-type association for each up-or down-regulated autophagy genes in the scRNA-seq datasets. Benjamini-Hochberg FDR adjustment was used for multiple tests correlation. For survival analyses, Up-autophagy scores and down-autophagy scores were divided into quartiles for categorization and the log rank test was used to calculate P-values. The Cox proportional hazards (PH) regression model was used to calculate the Hazard Ratio (HR), the 95% confidence interval (95% CI), and p values.